The Development of the Lung Vasculature in Congenital Diaphragmatic Hernia and Its Clinical Implications

Emrah Aydin

Universitat Autònoma de Barcelona

Doctoral Program in Surgery and Morphological Sciences

Department of Surgery

The Development of the Lung Vasculature in Congenital Diaphragmatic Hernia and Its Clinical Implications

Lung Vasculature in Congenital Diaphragmatic Hernia

Candidate: Emrah Aydin

Director: Jose Luis Peiro Ibanez

Tutor: Eloi Espin Basany

BARCELONA, 2024

Acknowledgements

Education is a lifetime journey. During this journey, you have the chance to meet many people. However, some of the people you met enlighten your way. Prof. Dr. Jose Luis Peiro Ibanez, whom I met in 2011 for the first time in Barcelona opened new frontiers in my life.

I would like to thank Prof. Dr. Eloy Espin Basany for his kind contribution and advice during my research.

I also would like to thank all the teachers and professors who had a powerful impact on my career.

Family is the backbone of the success of a person. Therefore, with the highest respect I would like to share my special thanks to my mother Gulistan Aydin, my father Hayri Aydin, my wife Pinar Ozge Avar Aydin and my little princess Kalben Aydin.

Dr. Emrah Aydin

Abbreviations

µCT	: Micro Computerized Tomography
aSMCs	: Airway Smooth Muscle Cells
BSA	: Body Surface Area
BW	: Body Weight
CDH	: Congenital Diaphragmatic Hernia
CT	: Computed Tomography
CVS	: Chorionic Villus Sampling
ECHO	: Echocardiography
ECMO	: Extracorporeal Membrane Oxygenation
ED	: Embryonic Day
EXIT	: Ex Utero Intrapartum Treatment
$FEF_{25–75}$	: Forced Expiratory Flow at 25%–75%
FEV_1	: Forced Expiratory Volume
GER	: Gastroesophageal Reflux
H&E	: Hematoxylin and eosin
KI	: Potassium Iodine
LMIC	: Low- and Middle-Income Countries
LW	: Lung Weight
MGI	: McGoon Index
MRI	: Magnetic Resonance Imaging
PAH	: Pulmonary Arterial Hypertension
PAI	: Pulmonary Artery Index
PBS	: Phosphate Buffered Saline
PFA	: Paraformaldehyde
PH	: Pulmonary Hypoplasia
PLUG	: Plug the Lung Until it Grows
PPHI	: Prenatal Pulmonary Hypertension Index
PPHN	: Persistent Pulmonary Hypertension in the Neonates
RAC	: Radial Alveolar Count
ROI	: Range of Interest
S/E	: Segment / Element Ratio
TLV	: Total Lung Volume

TO : Tracheal Occlusion

UCSF : University of California, San Francisco

USG : Ultrasonography

vSMCs : Vascular Smooth Muscle Cells

vWF : von Willebrand factor

WHO : World Health Organization

α-SMA : Alpha-Smooth Muscle Actin

Index of tables

Table 1: The stages of lung development. 7
Table 2: The connectivity matrix of the tree given in Figure 2 21
Table 3: Intervals for the ordering scheme 32
Table 4: The morphometric results per vessel type. (RPA: Right pulmonary artery, RPV: Right pulmonary vein, LPA: Left pulmonary artery, LPV: Left pulmonary vein, L/D ratio: Vessel length to diameter ratio.) (Values expressed as means ± standard deviations) 37
Table 5: Comparison of the lung morphometry 42
Table 6: The numbers of pooled segments and pooled elements 43
Table 7: Comparison of the mean number of segments and elements 43
Table 8: Comparison of the mean length of segments and elements 43
Table 9: Comparison of the mean S/E and L/D ratios 45
Table 10: Comparison of the mean of connectivity matrices 45
Table 11: U, p values for connectivity matrices 46

Index of figures

Figure 1: Creation of congenital diaphragmatic hernia with surgical technique in the sheep and tracheal occlusion with clips. (Figure was used with the permission of Prof. Jose Luis Peiró.)..... 15
Figure 2: The surgical model to create Congenital Diaphragmatic Hernia in rabbit. (Figure was used with the permission of Prof. Jose Luis Peiró.)..... 16
Figure 3: Oral administration of nitrofen to the pregnant rats and tracheal occlusion in rat fetuses with congenital diaphragmatic hernia. (Figure was used with the permission of Prof. Jose Luis Peiró.) 16
Figure 4: Order of segments according to the Strahler method..... 18
Figure 5: The elements formed by segment groups of the same order connected to the serial form are indicated by cut lines. The remaining singular segments are also defined as elements. 19
Figure 6: A tree with full branching symmetry for all levels 20
Figure 7: The flow chart of the study 27
Figure 8: The administration of the Lugol solution..... 28
Figure 9: A: Partially peeled skin of a rat fetus (arrow), B: Contrast enhancement of the fetus under micro-CT. 33
Figure 10: Embryos' micro-CT scans. A: The right ventricle is immediately injected with contrast material. B: The fetus' upper half of its body is immersed in Lugol solution. C: The skin is partially peeled off in option. 33
Figure 11: The vascular structures gathered through different Lugol applications. 34
Figure 12: Ex-vivo Lugol treatment on a partially excised skin specimen yielded three-dimensional pictures of the complete lung vasculature in the coronal and axial planes (A,B), Skeletonization of the entire lung vasculature (C), colored image allowing analysis of a single lobe's vasculature (D), and skeleton of a single network of vessels in the right lobe (E) with mapping, which aids in measuring all vessel parameters by either choosing the vessel junctions (blue [mid-branches] and red [end branches]) or the vessels themselves (yellow and green) (F). 34
Figure 13: Mapping of the tree structure 35
Figure 14: Rendered view of the tree structure of the lung vasculature 35
Figure 15: An example of a tree structure analysis 36
Figure 16: Strahler system with defined diameter [157]. 37
Figure 17: An illustration of ordered artery branches 37
Figure 18: The mean vessel number of each vessel type across generation groups. (RPA: Right pulmonary artery, RPV: Right pulmonary vein, LPA: Left pulmonary artery, LPV: Left pulmonary vein.)38
Figure 19: Hematoxylin and eosin staining of lungs from control and nitrofen-exposed fetuses at ED21. 38
Figure 20: Masson-Goldner staining of lungs from control and nitrofen-exposed fetuses at ED21. 39
Figure 21: Immunofluorescence staining of lung tissue from the control group at ED21 for alpha-smooth muscle actin (α-SMA). α-SMA staining was strongly seen in vascular smooth muscle cells (vSMCs, asterisks) surrounding pulmonary vessels and airway smooth muscle cells (aSMCs) surrounding bronchioles..... 40
Figure 22: Immunofluorescence staining of lung tissue from the control group at E21 for von Willebrand factor (vWF). 40
Figure 23: Protein expression levels of vWF and β-tubulin in loaded amounts of 60 µg and 40 µg of protein from lungs of control and nitrofen-exposed fetuses at ED21..... 41

Figure 24: Protein expression levels of α-SMA in loaded amounts of 60 µg and 40 µg of protein from lungs of control and nitrofen-exposed fetuses at ED21. 41
Figure 25: A: Micro CT scan of the fetal lung, B: Segmentation of the arterial vasculature, C: Segmentation of the venous vasculature, D: Skeletonized Right Artery 42
Figure 26: The link between the quantity of pooled elements and the order numbers for the left (A) and right (B) lungs, the length of pooled elements and the order numbers for the left (C) and right (D) lungs, the diameter of pooled elements and the order numbers for the left (E) and right (F) lungs. 44

Index

Summary 1
Introduction 1
Hypothesis 1
Materials and Methods 1
Results 1
Conclusion 2
Resum 3
Presentació 3
Hipòtesi 3
Materials i Mètodes 3
Resultats 3
Conclusió 4
1. Introduction 5
1.1. History of fetal surgery 6
1.2. Prenatal diagnosis 6
1.3. Lung development 7
1.3.1. Pulmonary hypoplasia 8
1.3.2. Pulmonary hypertension 8
1.4. Congenital diaphragmatic hernia 8
1.4.1. Prognostic factors in CDH 9
1.4.2. Treatment modalities in CDH 13
1.4.5. Outcome in CDH 14
1.5. Animal models in congenital diaphragmatic hernia 15
1.6. Mathematical modeling of lung structure in congenital diaphragmatic hernia 17
1.6.1. Segment / Element ratio 19
1.6.2. Connectivity matrix 20
1.6.3. Fractal geometry 21
2. Scientific justification 23
3. Hypotheses 25
4. Objectives 26
5. Materials and methods 27
5.1. Study design 27
5.2. Creation of CDH 27

5.3. Preparation of the fetuses 27
5.4. Specimen preparation 28
5.5. Micro-CT imaging 28
5.6. Image analysis 28
5.7. Data acquisition 29
5.8. Data processing 29
5.8.1. Segmentation 29
5.8.2. Nomenclature 29
5.8.3. Mapping of the tree structure 29
5.8.4. Connectivity matrix 30
5.9. Histological analysis 30
5.9.1. Hematoxylin & Eosin staining 30
5.9.2. Mason Goldner (Trichrome) staining 30
5.9.3. Immunofluorescence and Western Blot analysis 31
5.10. Statistical analysis 32
6. Results 33
6.1. Gross results 33
6.2. Visualization of fetal lung microvasculature 34
6.3. Morphometry 37
6.4. Histology 38
6.4.1. Hematoxylin and Eosin staining 38
6.4.2. Masson-Goldner staining 39
6.4.3. Immunofluorescence staining 39
6.4.4. Western Blotting 40
6.5. Group comparison 41
6.5.1. Comparison of total networks 42
6.6. Results of tree structure mapping 42
6.7. Results of connectivity matrix 45
7. Discussion 47
8. Conclusions 50
9. Future lines 51
10. Bibliography 52

Summary

Introduction

Congenital diaphragmatic hernia (CDH) is seen at 1 in every 2500 live births. Its overall mortality is still as high as 50% regardless of the improvements in the management of neonates in the intensive care units. Pulmonary hypertension and underdevelopment are the primary causes of death in CDH. CDH has typical microscopical findings of a decreased number of alveolar branches; lessened alveolarization; decreased compliance and the pulmonary arterioles' muscle layers' thickness has increased. The incomplete development of the diaphragm causes herniation of the abdominal organs, such as the intestines, stomach, spleen, and in severe cases liver into the thoracic cavity. At that point, competition for space is established in the thoracic cavity, generating compression of the fetal lung tissue and egression of the essential intrapulmonary fluid that leads to the arrest of normal fetal lung development. Per our current knowledge, the severity of the CDH could be predicted by the ratio of ipsilateral lung area to head circumference, total lung volume, left/right ventricle ratio, modified McGoon index, location of the stomach with the existence of polyhydramnios, and the location of the liver. When the blood pressure in the pulmonary system exceeds 2/3 of the pressure in the systemic circulation, it is said to be pulmonary hypertension. Although the main pathology emerged in utero, this could only be documented by echocardiography in the early neonatal period. This is mostly because the blood flow into the lungs is limited in utero for the sake of fetal blood circulation. This is a significant barrier for treating CDH patients in-utero. Moreover, even in echocardiography, the finding of tricuspid regurgitation jet velocity, a measure of pulmonary hypertension, aids the estimation of pulmonary artery pressure, it was not successful in predicting the severity of pulmonary hypertension. Nonetheless, the aberrant organization of the pulmonary vascular network in pulmonary hypertension can only be shown in postmortem subjects by histopathological analyses.

Hypothesis

Since pulmonary hypertension is one of the predictors of the survival of these patients, this proposal seeks to test the general hypothesis that a prenatal pulmonary vascular branching index correlates with the severity of postnatal pulmonary hypertension.

Materials and Methods

Sprague Dawley rat fetuses that were both healthy and nitrofen-induced were used. The fetuses underwent micro-computed tomography scanning. Using artificial intelligence techniques, the pulmonary artery tree was 3D reconstructed. Moreover, a framework is developed to generate 3D pulmonary vascular tree structures by using Computed Tomography (CT) scans. Then, the developed framework is used to compare pulmonary vascular trees of CDH samples and healthy controls to determine the characterization of the CDH disease. Finally, by using pulmonary vascular trees, morphological features are obtained, and characterization of the disease is achieved.

Results

There were 70 fetuses examined throughout the study, 40 of which were used in the first part to demonstrate the feasibility of the Lugol application while the rest were used in the second part. Lugol diffused uniformly throughout the capillaries in the pups with partially removed skin, allowing fine-grained imaging of the lung vasculature. The segmentation part of this project had 86% precision, 82% sensitivity, and 84% F1 score. For the characterization of the CDH, the required features are obtained from the

segmented output, and they were prioritized by their impact on the classification. The number of segments in CDH was significantly lower than the control group on the left (U=2.5, p=0.004) and right (U=0, p=0.001) sides for order 1(O1), whereas there was a significant difference only on the right side for O2 and O3. The pooled element numbers in the control group obeyed Horton's Law (R^2=0.996 left and R^2=0.811 right lungs), while the CDH group broke it. Connectivity matrices showed that the average number of elements of O1 springing from elements of O1 on the left side and the number of elements of O1 springing from elements of O3 on the right side were significantly lower in CDH samples.

Conclusion

Lung vasculature in CDH is of particular interest for pulmonary development and is the main underlying factor that determines the disease severity. We observed that, besides the known reduced airway branching of the hypoplastic lungs, arterial branching was decreased in fetuses with CDH as well. Herein, we have demonstrated that the radiological imaging techniques were able to define the prenatal lung vascular tree, which could potentially estimate the degree of pulmonary hypertension and enable physicians to determine the severity of the disease prenatally and promote prenatal therapy.

Resum

Presentació

La hernia diafragmàtica congènita (HDC) es veu en 1 de cada 2500 naixements vius. La seva mortalitat global és tan alta com el 50% malgrat les millores en el maneig dels neonats a les unitats de cures intensives. El subdesenvolupament i la hipertensió pulmonar són les causes principals de mort en l'HDC. Aquesta malformació presenta trets microscòpics típics com son una disminució del nombre de branques alveolars; menor alveolització; disminució de la compliància i l'augment de l'espessor de les capes musculars dels arteriòls pulmonars. El tancament incomplet del diafragma causa la herniació dels òrgans abdominals, com els intestins, l'estómac, la melsa i, en casos greus, el fetge cap a la cavitat toràcica. En aquest punt, s'estableix una competència per l'espai a la cavitat toràcica, generant la compressió del teixit pulmonar fetal i l'egressió del essencial fluid intrapulmonar que porta a la detenció del desenvolupament pulmonar fetal normal. Segons el nostre coneixement actual, la gravetat de l'HDC es pot predir per la relació entre l'àrea del pulmó contralateral i el perímetre cranial, el volum pulmonar total, la relació ventricle esquerre/dret, l'índex de McGoon modificat, la localització de l'estómac, l'existència de polihidramni i la localització del fetge. Quan la pressió sanguínia en el sistema pulmonar supera 2/3 de la pressió en la circulació sistèmica, es diu que hi ha hipertensió pulmonar. Encara que la patologia s'origina in utero, això només es pot documentar per ecocardiografia al període neonatal precoç. Això és majoritàriament perquè el flux sanguini cap als pulmons està limitat in utero per causa de la circulació sanguínia fetal. Això representa una barrera significativa per al tractament de pacients amb HDC in utero. A més, fins i tot en l'ecocardiografia, el calcul de la velocitat del jet de regurgitació tricúspide, una mesura de la hipertensió pulmonar, ajuda a l'estimació de la pressió arterial pulmonar, no va tenir èxit en predir la gravetat de la hipertensió pulmonar. No obstant això, l'organització aberrant histológica de la xarxa vascular pulmonar en la hipertensió pulmonar només es pot mostrar en subjectes post mortem mitjançant anàlisis histopatològics.

Hipòtesi

Donat que la hipertensió pulmonar és un dels predictors de la supervivència d'aquests pacients, aquesta proposta busca provar la hipòtesi general que un índex de branquificació vascular pulmonar prenatal correlaciona amb la gravetat de la hipertensió pulmonar postnatal.

Materials i Mètodes

Es van utilitzar fetus de rates Sprague Dawley tant control sans com induïts amb nitrofen per generar HDC. Els fetus es van sotmetre a escaneig per tomografia computada microscòpica. Utilitzant tècniques d'intel·ligència artificial, l'arbre de l'artèria pulmonar va ser reconstruït en 3D. A més, es va desenvolupar un marc per generar estructures d'arbre vascular pulmonar en 3D utilitzant escaneigs per Tomografia Computada (TC). Després, el marc desenvolupat es va utilitzar per comparar arbres vasculars pulmonars de mostres d'HDC i controls sans per determinar la caracterització de la malaltia d'HDC. Finalment, utilitzant arbres vasculars pulmonars, es van obtenir característiques morfològiques, i es va aconseguir la caracterització de la malaltia.

Resultats

Es van examinar 70 fetus durant l'estudi. D'aquests, 40 es van utilitzar en la primera part per demostrar la viabilitat i eficacia de l'aplicació de Lugol mentre que la resta es van utilitzar en la segona part. Lugol es va difondre uniformement a través dels capil·lars en els neonats amb la pell parcialment resecada, permetent la imatge de gran detall de la vasculatura pulmonar. La part de segmentació

d'aquest projecte va tenir una precisió del 86%, una sensibilitat del 82% i una puntuació F1 del 84%. Per a la caracterització de l'HDC, es van obtenir les característiques necessàries de la sortida segmentada, i es van prioritzar segons el seu impacte en la classificació. El nombre de segments en l'HDC va ser significativament inferior al grup control a l'esquerra (U=2.5, p=0.004) i a la dreta (U=0, p=0.001) per a l'ordre 1(O1), mentre que només hi va haver una diferència significativa a la banda dreta per a O2 i O3. Els números d'elements agrupats en el grup de control obeïen la Llei de Horton (R2=0.996 pulmons esquerres i R2=0.811 drets), mentre que el grup d'HDC no la va complir. Les matrius de connectivitat van mostrar que el nombre mitjà d'elements d'O1 que brollaven d'elements d'O1 al costat esquerre i el nombre d'elements d'O1 que brollaven d'elements d'O3 al costat dret eren significativament inferiors en mostres d'HDC.

Conclusió

La vasculatura pulmonar en l'HDC és d'interès particular per al desenvolupament pulmonar i és el principal factor subjacent que determina la gravetat de la malaltia. Hem observat que, a més de la coneguda reducció de la branquificació de les vies respiratòries dels pulmons hipoplàstics, la branquificació arterial també va disminuir en fetus amb HDC. Aquí, hem demostrat que les tècniques d'imatge radiològica van poder definir l'arbre vascular pulmonar prenatal, el qual podria potencialment estimar el grau d'hipertensió pulmonar i permetre als metges determinar la gravetat de la malaltia prenatalment i millorar la teràpia prenatal.

.

1. Introduction

In the last 30 years, there have been tremendous efforts in order to decrease children's death. The number of deaths under the age of five decreased from 12.5 million in 1990 to 5.3 million in 2018 [1]. However, the decrease in neonatal deaths is much slower which was 2.4 million in 2019 [1,2]. Moreover, the ratio of death under the age of five is 46% [2]. In the meantime, since death due to infectious causes declined, the ratio due to congenital anomalies has risen. There are around 303,000 neonatal deaths yearly due to congenital anomalies while almost half a million deaths under the age of five [3–5]. Global Burden of the Diseases Study stated that congenital anomalies are the fifth most common cause of death under the age of five and the 11th most common cause of death in all age groups [6,7].

The World Health Organization (WHO) describes congenital abnormalities as the constitutional and functional problems of the baby that happen in utero. It affects 3-6% of live births worldwide [3]. Countries with low and moderate incomes (LMIC) per the criteria of the World Bank have the highest incidence of congenital anomalies mostly due to inadequate maternal nutrition, teratogens, prenatal infections, and inadequate prenatal diagnosis [8]. It is assumed that more than 95% of deaths due to congenital anomalies are hosted by LMICs [4]. Sustainable Developmental Goals 3.2 by the United Nations aims to stop preventable deaths of neonates and patients under the age of five by 2030 [9].

"*Doctor, may I have a normal baby?*" [10]. Many doctors encounter this question through their practice. "The normal" mostly refers to a healthy or above average baby while a few times refer to babies without congenital anomalies. Plato was the first one who define this condition while Francis Galton was the first one who define the term "eugenic" (Greek: *eu-genēs*: good-born). The term stands for the science to enhance the quality of the newborn and get the most advantageous characteristics. In time, it has had different interpretations under various rulers. There were certain points where science and politics met with each other while some others that both stood at different edges which resulted in the loss of many lives. In 1946, WHO declared the definition of health for the first time and revised it in 1948 for the last which brings eugenic in a scientific, humanistic, and ethical format. According to this definition, *health is a state of complete physical, mental, and social well-being and not merely the absence of disease or infirmity*. Therefore, the birth and the development of prenatal management strategies aimed at the same idea. Especially in developed countries, to decrease the incidence of congenital anomalies various precautions are taken such as education before intercourse, adequate and necessary nutritional support during pregnancy, and the use of prenatal screening and treatment strategies. The screening strategies have been improved from invasive to noninvasive ones in time [11]. The aim is not to demolish the unhealthy babies but to find them as early as possible and prevent any possible damage if possible or if not to lessen the negative impact and keep them alive in the most possible way.

Fetal surgery enables the treatment of many congenital problems to be treated in utero. However, the diagnostic process is still painful. It necessitates a special education and experience. Moreover, the specific limitation of the diagnostic procedures and tools that could be used in utero even worsens the situation. The error rates are still higher than expected [12,13]. Time limitations and technical issues put additional disadvantages on imaging modalities which indeed results in unnecessary use of additional diagnostic tools or consultations, therefore increasing the workload and cost in the patients, physicians, and healthcare systems.

1.1. History of fetal surgery

There have been tremendous efforts to improve prenatal diagnosis in accordance with the improvement in technology. As our understanding of the development of the fetus and the mechanism of the disease improves, new techniques for in-utero treatment become available [14]. While Embryological renderings of the fetus in the womb by Leonardo Da Vinci was the first, Vesalius was the first who published fetal anatomy in his well-known work "De Humani Corporis Fabrica libri septem" in the 16th century (1543), which are the oldest known studies on fetus [15,16] After Vesalius, Bichat made the first study on the movements of the fetus in 1803; Zuntz in 1877 and Preyer in 1885 showed in their studies that the fetus should be kept in warm serum and that if it breathes, it is not possible to continue the pregnancy. While Mayer and Swenson performed the first successful fetal intervention in animals in 1920, Nicholas demonstrated normal delivery for the first time after fetal intervention [17]. Following that, between 1960 and 1970, animal disease models were developed, and in the 1980s, some treatment methods were developed [18–25]. Intrauterine transfusion performed in New Zealand for Rh incompatibility has taken its place in history as the first fetal intervention in humans [17]. This was followed by the first diagnostic fetoscopy in 1974, followed by the first open fetal surgery in 1983 by Michael R. Harrison, a professor at the University of California, San Francisco (UCSF), who led the group.

With the increase in experience over time, many diseases in the fetal period have become treatable. Thus, fetal surgery offers an alternative to families in case of a disease diagnosed in the prenatal period other than terminating or waiting for birth. However, as in the development process of all branches of medicine, fetal surgery also follows a fluctuating course while continuing its development. Its popularity in the beginning years was stalled due to the early results not being as good as expected, and it started to gain popularity again with endoscopic intervention opportunities and the developing medical support systems. Unfortunately, this popularity also brought different risks or negativities [26,27]. To overcome this, it is necessary to master the current treatment approaches as well as these diseases [28]. In this way, it will be possible to use the appropriate intervention on the appropriate patient at the appropriate time using the appropriate technique.

1.2. Prenatal diagnosis

While evolving to industry 5.0 from industry 4.0, today, the most frequently used diagnostic method in pregnant women continues to be ultrasonography (USG) with its relatively high reliability, easy accessibility, and low cost. There may be differences in the results depending on the user, and it is also affected by the factors related to the patient. The use of high-frequency USG, on the other hand, causes the possible side effects on the fetus to be questioned [29,30]. Due to the presence of unmeasurable side effects, the structural examination of pregnancies without a suspected congenital anomaly should be performed on the 18th-22nd week. Doppler studies during these prenatal USG allow us to precisely analyze the fetal hemodynamics and the heart anatomy and function in the fetal echocardiography. The second most commonly used diagnostic method in the fetal period is magnetic resonance imaging (MRI). Fetal MRI is superior to USG in revealing congenital anomalies. However, although it lags behind USG due to the need for specialists who can evaluate as much as the cost of shooting and device, it is increasingly used in centers in Europe and America. Fetal echocardiography (ECHO) is used in the screening and detailed examination of congenital heart anomalies, that not rarely are associated or consequence of the compression secondary to the CDH. If an anomaly is suspected in the fetus, an aneuploidy test can be

performed after the 9th gestational week, CVS sampling after the 11th gestational week, or amniocentesis after the 15th gestational week.

1.3. Lung development

The lung is the main organ for respiration, which is spongy, air-filled, and located on either side of the chest. Lung development can be examined in two main parts: structural and functional. While structural growth is mostly mediated by physical factors, functional growth is a biochemical process predominantly controlled by hormones [31]. Structural growth continues throughout pregnancy. The branching of the airways continues and the formation of alveoli, where air exchange takes place, occurs in the last trimester of pregnancy. However, lung development continues in the form of an increase in the number of alveoli even after birth. At the end of the development process, a structure with a surface area of 50—100 m2 that allows the process of carbon dioxide and oxygen exchange is formed.

Structural and functional development of the lung is possible with the successful completion of the physical and biochemical development of the lung [32]. While the lung provides its structural integrity at the end of the physical development process, this structure with a large surface area becomes stable with the formation of surfactant after biochemical processes. These two processes are completed in coordination with each other. Failure in any of these two processes results in insufficiency of the newborn's lung capacity or respiratory system.

Lung development occurs in five stages (Table 1). The times of these stages can vary between fetuses, and there are also transitions between stages. The reason why no consensus has yet been reached on the specified weeks is due to this.

Table 1: The stages of lung development.

Embryonic	3-7. weeks	Lung budding occurs. Trachea and bronchial differentiation are seen.
Pseudo-glandular	7-17. weeks	The airways continue to branch, and terminal bronchioles are formed. Respiratory bronchioles and alveoli are not yet present.
Canalicular	17-27. weeks	Terminal bronchioles divide into two or more respiratory bronchioles. These are further subdivided into three to six alveolar ducts.
Saccular	27-36. weeks	Terminal sacs (alveolar precursors) begin to form, and capillaries appear around them.
Alveolar	36. week – 10 years	Mature alveoli form epithelial – endothelial connections with capillaries.

In the third week of pregnancy, the lung bud originates from the foregut. During this period, the buds of both lungs are developing. By the fifth week, both primary lung buds are recognizable. After this stage, the second branching occurs. Lobar buds begin to appear, three on the right and two on the left. From these buds, the lobes of the lungs are formed. By the eighth week, lobar buds continue to segment, and bronchopulmonary segments are formed. In the pseudo-glandular stage, the airways which are responsible for conduction occur. Towards the end of this phase, primitive airlines, consisting of 16-25 generations, occur. By the sixteenth week, the bronchi complete their formation, and the tree structure lengthens and expands. In the canalicular stage, the structures of the lungs responsible for gas exchange occur.

1.3.1. Pulmonary hypoplasia

Pulmonary hypoplasia (PH) in children, especially in newborns, is a rare diagnosis that has high mortality and morbidity [33–39]. It is characterized by small, underdeveloped lungs and may have serious effects on the child's development. The majority of the cases resulted from problems that happened during pregnancy such as oligohydramnios or premature rupture of membranes [40]. Another main cause is the congenital anomalies that have the potential to cause severe respiratory insufficiency. Due to the fact that airways form in parallel with the lung vasculature, it is mostly presented with pulmonary arterial hypertension (PAH). The Askenazi-Perlman was aimed to define PH. If the lung weight (LW) / body weight (BW) ratio is less than 0.009 it indicates PH. If the LW/BW ratio is over 0.018, the likelihood of PH is extremely limited. Between these values, radial alveolar count (RAC) is used to determine the diagnosis.

1.3.2. Pulmonary hypertension

High blood pressure in the pulmonary system is referred to as pulmonary hypertension which affects the arteries of the lung and the right side of the heart. Blood vessels are narrowed mostly when compared with the normal ones while they may also be blocked or destroyed. This pathology indeed slows down the flow in the pulmonary vasculature resulting in an increase in the pressure at the walls of vessels, mainly arteries. In healthy newborns, pulmonary system blood pressure decreases half of the systemic blood pressure in the postnatal 12th hour, 1/3rd in the 24th hour, and to the adult values in 2-6 weeks. It is defined as the pulmonary arterial blood pressure being higher than 2/3 of systemic pressure. Pulmonary blood pressure values between 26-35mmHg in the postnatal period with echocardiography are classified as mild PAH, between 36-45mmHg as moderate PAH, and above 45mmHg as severe PAH.

The main determinants of the outcome in PAH are the capacity of the respiratory circulation and the degree of resistance in vasculature. It is already known that the status of the pulmonary system correlates with the level of lung remodeling [41]. The defective fetal lung histology with aberrant vascularity causes PAH to be more severe. PAH is the most important factor affecting the morbidity and mortality of CDH patients [42,43]. Although the main pathology begins in utero, PAH can only be proven postnatally after the newborn starts to breathe. Hypoxia exacerbates vascular reactivity and PAH. Decreased airway branching, decreased compliance, and thickened muscle layers of pulmonary arterioles are seen in these patients' lungs [44]. The amount of prenatal intrapulmonary blood flow is lower when compared to the postnatal period due to the difference in the anatomy and physiology of circulation in utero and after birth. Although the arterial vessel wall thickness has increased, the low amount of blood causes a lower pressure on the vessel wall, therefore making the prenatal diagnosis almost impossible. With the cascade of physiological events that occur during and after birth, the blood flow through the lungs increases, thus the intrapulmonary blood pressure values rise above normal.

1.4. Congenital diaphragmatic hernia

An embryological failure in the correct fusion of pleuroperitoneal membranes to form an intact and closed diaphragm that separates the chest and abdomen, known as congenital diaphragmatic hernia (CDH), does cause abdominal organs to migrate into the thoracic cavity. This condition puts a major obstacle in the development of the lungs that become compressed due to the competition for space in the chest. It may be isolated or be a part of a syndrome. The reported incidence of the disease varies but has a range between 0.8 - 5/10,000 births or 1 in 2500-3000 live births [45–49]. Male gender has a slightly

higher tendency while African Americans have a lower risk of isolated CDH [49,50]. While left-sided defect is more common in CDH, it can occur on either side or bilaterally. The underlying pathophysiology of CDH could not be determined yet as well as the inheritance pattern. The diagnosis could be done during a routine prenatal USG in the first and second trimester. CDH has long been regarded as a difficult medical and surgical condition in pediatric patient groups. The statement "*For the patient in whom the hernia makes its appearance at birth, little or nothing can be done from a surgical standpoint*." by Greenwald and Steiner has evolved in time [51]. Ladd and Gross performed the first successful repair of CDH just in the next decade [52]. There are many centers and researchers that continue to investigate the etiology of the disease. The abdominal organs that herniate into the thoracic cavity put pressure on the lungs and cause the lungs to remain small and underdeveloped which is defined as pulmonary hypoplasia. In some of these patients, various organs might be affected including heart, liver, intestines, and nervous system development. Regardless of the innovations in technology, the survival and quality of life are still below expectations [53–56]. However, diaphragmatic flaw repair that was put off, extracorporeal membrane oxygenation (ECMO) usage in predetermined patients, fetal intervention during pregnancy, sophisticated ventilator strategies preventing barotrauma, and improvements in the management of newborns decreased the mortality in these patients [57]. On the other hand, many patients with severe CDH continue to have a higher rate of morbidity and mortality. Therefore, the status of the CDH patients can range from mild to severe. In the best of scenarios, infants' general status is so well that they do not necessitate a prenatal intervention or emergency intervention just after birth. While regardless of the severity of the disease, the lungs are smaller than the babies in the same gestational week, they still could catch up and adapt after some time. But given their protracted hospital stays and the requirement for a multidisciplinary approach to their management and follow-up beyond hospital discharge, it's all but a requirement. Numerous long-term health concerns with breathing, nutrition, growth, hearing, and development affect these infants. The overall mortality of newborns with CDH is 40-50% [45,58,59]. Rather than the abnormality itself, hypoplasia of the lungs and pulmonary hypertension are to blame for CDH-related mortality. Even though several theories have been presented to explain pathophysiology, no study presents the exact etiology. Even if the defect is repaired, children may be lost due to lung problems. Moreover, both lungs are shown to be damaged by the influence of genetic or environmental factors during development.

1.4.1.Prognostic factors in CDH

There are numerous prenatal requirements, proposed to define the severity of the case and to select those patients that could be operated on in utero, in the literature [45]. The lung-to-head ratio (LHR), the observed to expected LHR (O/E LHR), the total lung volume (TLV), the observed to expected (O/E TLV), McGoon Index, the herniation of liver and the presence of hernia sac are among the most accepted ones.

1.4.1.1. Lung-to-Head ratio

LHR has been suggested by numerous writers as a CDH prognostic factor. The LHR is calculated with the area of the lung contralateral to the defect, as the ipsilateral many times is not detectable, divided by the circumference of the fetal head, as assessed by ultrasonography in the 4 chambers view chest axial section. The head circumference is the biometric parameter used to homogenize and correct the natural variability and differences in the size of different fetuses. In the original report of this method, the

area of the right lung was measured at 25 weeks' gestation in fetuses with left-sided CDH and intrathoracic liver herniation [60]. When inspecting the four-chamber picture of the heart in the thorax's cross-sectional plane, by dividing the lung's largest diameter by its largest perpendicular diameter, the right lung's area was estimated. But to calculate the lung area, the anteroposterior lung diameter at the mid-clavicular line was multiplied by the perpendicular diameter at the midpoint of the anteroposterior diameter. Nowadays the tracing method for area calculation is preferred. The authors of that study also tried to develop a gestation-neutral assessment, as the LHR increases with gestational age, and compared this LHR with the expected in a normal fetus at those gestational ages. With that, it becomes more useful to calculate the O/E LHR (observed to expected LHR). Due to the extensive range of gestational ages at which the LHR was measured, the few patients that were evaluated in the majority of research, and the usage of LHR being extended from patients with left-sided CDH and intrathoracic liver to those with right-sided hernia and those without liver herniation may all be contributing factors to the significant discrepancies in reported results. With routine postnatal treatment, it is believed that the death rate for fetuses with CDH with intrathoracic liver herniation, sometimes known as "liver-up" instances, is significant, as we demonstrated in our series. For further risk stratification of potential candidates for fetal surgery, LHR has been employed in conjunction with instances that have been labeled as "liver-up" cases. [45,61–63]. In-utero intervention entails obliteration or blockage of the fetal trachea (also known as "plugging"), which was once accomplished through open surgery (using metallic clips) and is now accomplished through endoscopic procedures using endoluminal balloons [61–65] Plugging has been linked to a variety of consequences. The use of LHR criteria by diverse scientists to choose those who will benefit from prenatal intervention may have influenced the findings. Various researchers have supported and questioned LHR's effectiveness as a prognostic indicator since it was originally identified in 1995 [60,66,67]. Quintero and colleagues argue that both the observed/expected LHR and the LHR are independent of pregnancy age theoretically, and hence should be used with caution in predicting newborn outcomes [68].

With the current knowledge, LHR should be calculated using the following standards.

1. The heart should be viewed axially from the perspective of the four chambers.
2. The herniated tissues in the image should be farther from the probe than the unaffected lung.
3. You can prevent shadows cast by the costa by placing the transducer so that the ultrasonic beam spans the intercostal gap and is parallel to the costa.
4. The picture must be frozen before applying the maximum magnification to make sure every landmark is discernible. Then, it should be enlarged until the fetal thorax's axial view occupies the entire screen.

Another limitation of the LHR is that LHR sonographic assessment (using areas) is less accurate than MRI which measures lung volumes [69]. Furthermore, both lungs can be evaluated using MRI which is simpler to standardize. Finally, if continuing trials show that PLUG is effective, more of the affected fetuses might be handled in specialized clinics in which MRI would be the primary technique for determining the severity of the disease. Since USG is available in all centers and easy to use weekly, still O/E LHR is considered the gold standard for evaluating candidates for FETO and to do the postoperative follow-up.

1.4.1.2. Total Lung Volume

The known nomenclature for lung volumes refers to respiratory volumes which consist of tidal volume, inspiratory reserve volume, and expiratory reserve volume. However, when it is related to CDH, it refers to the volumes of the fetal lung measured by fetal MRI. Imaging is critical for assessing the lung antenatally, estimating the prognosis, and deciding on a follow-up approach. Although ultrasonography helps diagnose CDH, it can only provide limited information due to a variety of maternal, fetal, and technical issues. MRI, on the other hand, is recognized to provide more precise and thorough information regarding fetal anatomy. Compared to USG, fetal MRI picture quality is almost unaffected by oligohydramnios, fetal malposition, or maternal obesity. Furthermore, FLV values in MRI have been shown to have high accuracy and reliability, while having very low variations between observers [70]. MRI has been proposed as a tool for detecting prognostic variables linked to the degree of pulmonary hypoplasia [71,72]. Total lung volume (TLV) is a measure of pulmonary hypoplasia in CDH that is calculated using MRI [73–76]. Fetal TLV can be measured on MRI using a variety of approaches. The freehand ROI can be used to delineate the lung parenchyma on each slice and multiplied by the slice thickness [72,77]. The mediastinal volume is subtracted from the total thoracic volume to calculate the fetal TLV [76]. Rypens et al. and Meyers et al. provided methods for estimating predicted fetal TLVs adjusted for gestational age using MRI measurements [72,77]. Büsing et al. found a high association between the FLV and ECMO need after the 30th week of gestation using logistic regression analysis. Of 95 fetuses investigated, the mortality was 70.8% under 5ml of FLV while the mortality was 0.3% under 25ml FLV. The same patients ECMO need was 56% who had FLV less than 5ml while it was 8.7% in patients with 40ml FLV [70]. Kastenholz et al. demonstrated in their study that TLV correlates with the outcomes for left-sided CDH while no correlation could be shown with right-sided CDH [71].

1.4.1.3. McGoon Index

Angiographic measures of pulmonary artery size are routinely employed in the investigation of congenital heart disease to predict outcomes before surgical treatment of obstructive right-heart defects [78,79]. It can estimate pulmonary hypoplasia indirectly, that is, based on the proportion of the diameters of the two pulmonary arteries at the hilus level and the descending aorta where it crosses the diaphragm which is the so-called modified McGoon Index. It is shown to be correlated with preoperative predictors of various diseases affecting the pulmonary system as well as postoperative follow-up and mortality [80–82].

Many studies in the literature indicated that MGI scores were good predictors of death in CDH neonates while there were discrepancies in the cutoff values [83–85]. Since MGI is measured via echocardiography the deviation between measurements of descending aorta varies. Furthermore, it was found that the width of the descending aorta in CDH infants was not substantially related to the body surface area of the infant. As a result, the authors stated that the diameter of the descending aorta in CDH neonates is not an appropriate variable for standardizing pulmonary artery size [83].

1.4.1.4. Pulmonary artery index

The pulmonary artery index, which is also known as the Nakata index, is calculated by dividing the total cross-sectional area of the pulmonary arteries by the total body surface area (BSA). It was first defined by Nakata et al. for the Fontan repair [79]. PAI scores were found to be good predictors of death in CDH neonates by Takahashi et al. [83]. Furthermore, their findings show that PAI can be used to predict

the degree of disease in survivors. Vuletin et al. demonstrated that prenatal PAI also can predict postnatal PAH in CDH patients and they named it as Prenatal Pulmonary Artery Index [86]. Since the BSA could not be determined in utero, the craniocaudal length of the vermis of the cerebellum, which enables the standardization for gestation age in the Prenatal Pulmonary Hypertension Index (PPHI) calculation, was obtained using midline sagittal scans of the brain. The PPHI was estimated by multiplying the diameter of the left pulmonary artery by the length of the cerebellum by ten.

1.4.1.5. Liver herniation

An earlier gestational age at diagnosis, a greater requirement for ECMO, and a slower rate of fetal lung development were all associated with liver herniation into the thorax, as previously reported in the literature [87–92]. In patients with liver up, the need for ECMO might change from 52.4% to 80% [45,92]. In left-sided CDH patients, the thoracic herniation of the liver usually implies a major diaphragm defect with abdominal organs herniating early, culminating in severe pulmonary hypoplasia and pulmonary hypertension. Even with advances in neonatal care, thoracic herniation of the liver continues to have a deleterious impact on survival. Also, mild herniation has a substantial impact on longevity and the requirement for ECMO. It is critical to measure the quantity of herniated liver when estimating prognosis because it was identified significant disparities in outcomes when comparing parts that herniated [45]. According to the literature, utilizing MRI to measure the proportion of the liver's herniated volume to the total volume of the thoracic cavity (LiTR) enabled independent assessment of postnatal outcomes from O/E TLV [93]. The best method for predicting death and the ECMO necessity in babies with isolated CDH is a combination of MRI, O/E TLV, and the proportion of liver herniation [94]. Furthermore, many studies have shown that early infant morbidity, the need for diaphragmatic replacement techniques, greater oxygen requirements, and a longer hospital stay are all predicted by liver herniation [87–92,95].

1.4.1.6. Presence of hernia sac

The parietal layer of the peritoneum and lung pleura form a hernia sac, which has been documented in 20% of instances in the literature [96]. However, research on the importance of the sac is limited, albeit all of them link the correlates of the sac with increased lung capacity and improved survival [97–99]. The prevalence of a sac was documented as 13.8% in a previous study done by our team, and it does not appear to be altered by the mother's age or the baby's gender [45]. The appearance of a sac in CDH is thought to confirm the late herniation, according to the studies already published in the literature [87]. When a hernia sac was present, the age of diagnosis was greater. CDH with an intact sac had greater fetal pulmonary development measures throughout the pregnancy. The hernia sac was the most important determinant in predicting the low necessity for ECMO cannulation and the patients' survival. The favorable effect of the sac presence also revealed a statistically significant difference in the length of stay in the hospital.

1.4.2. Treatment modalities in CDH

1.4.3. Prenatal management

1.4.3.1. Fetal Endoluminal Tracheal Occlusion - FETO

Harrison et al. described the initially called PLUG (Plug the Lung Until It Grows), a brief fetal tracheal occlusion that can correct pulmonary hypoplasia in CDH, in 1996 [61]. In a study of CDH lambs, Papadakis et al. found that the system that produces surfactants experienced improved parenchymal growth and maturation as a result of temporary tracheal closure. [100]. Kitano et colleagues investigated the effects of plug in rodents, speculating that pressure in the airways and secondary mechanical forces are the key cues for tracheal occlusion-induced lung expansion [101]. Harrison et colleagues used the PLUG approach on eight human babies ranging in gestation from 25 to 28 weeks [61]. They declared the obstruction in the prenatal lung via controlled tracheal blockage could grow underdeveloped lungs, even replace the abdominal viscera, and enhance postnatal pulmonary performance. The trachea was plugged with a foam plug or a titanium clip. A positive pulmonary response was seen in five of the patients. There were three failures, all of which were caused by the plug or clip not completely occluding the trachea.

1.4.3.2. Ex Utero Intrapartum Treatment - EXIT

Ex Utero Intrapartum Treatment (EXIT) is a successful treatment for reversing blockage at birth [102]. EXIT, which has a diverse staff and offers a regulated setting for protecting the airway, can unplug the trachea. The major goals of EXIT are to maintain fetoplacental circulation by securing the infant's airway via hysterotomy when the lower body and umbilical cord are left in the uterus while just the head and shoulders of the fetus are exteriorized. Ventilation could be achieved through orotracheal intubation or tracheostomy, the plug or clip could be removed or tracheoplasty could be performed prior to the chord clamping. This technique has already been shown to be both safe and effective [103]. Nowadays, the tracheal balloon is removed by a scheduled second fetoscopy, but sometimes labor starts before the planned date, and the tracheal occlusion should be reverted (balloon removal and intubation on placental support) by means of an EXIT procedure, just before delivery of the patient.

1.4.4. Postnatal management

It was Bochdalek from Prague who first described the posterolateral diaphragmatic defect in 1848 while Ladd and Gross were the first successors who treated the patients [104]. Since then, a lot has changed in the management of the patients. The CDH Europe consortium consensus in 2015 updated its protocol for the standardized management of CDH infants [105]. It can be summarized as planned delivery in a hospital with a large patient volume after 39 weeks' gestation; avoiding neuromuscular blocking agents during initial delivery room treatment; achieving preductal saturation of 80 to 95% and post-ductal saturation of >70% by modifying the treatment; targeting PaCO2 of 50 to 70mmHg; and the optimal initial ventilation method which is conventional mechanical ventilation, and newborns with CDH may benefit from intravenous sildenafil or other medications, anti-PAH as bosentan or epoprostenol. The use of inhaled nitric oxide is frequent, but its efficacy is controversial.

Regardless of the studies and reviews in the literature, there is still no consensus about the timing of the delivery. There are studies that show the mortality decreases with delivery at the later stages of the gestation while there are others that demonstrated the inverse correlation of the gestational age at the delivery and the ECMO need [106,107]. To complicate it, there are also studies that could not find any correlation between delivery age and survival [108].

As a standard of treatment, it is recommended that newborns with prenatally diagnosed CDH should be intubated immediately [105]. End-tidal CO_2 monitoring should be used to validate the location of the endotracheal tube. Low peak pressures, preferably less than 25 cm H2O, which decrease lung injury to the ipsilateral and contralateral lungs are recommended.

Patients with CDH have systemic hypotension, mostly correlated with the degree of pulmonary hypertension. Right-to-left shunting may be reduced by increasing systemic blood pressure. If the preductal saturation remains above 80%, blood pressure may be kept at its current levels. As a result, if preductal saturations remain between 80 and 95%, the consortium suggests maintaining arterial blood pressure at normal values for gestational age. On the other hand, surfactant therapy is unnecessary in this group since its quantities are anticipated to be proportional to pulmonary volume [109].

Once hemodynamic stability is established the type of surgery is to be determined. As of now, CDH is a physiological emergency, not a surgical one. The current controversies are also valid for the timing of surgery and optimal surgical technique. While some studies in the literature found that surgical repair following ECMO resulted in better results, others discovered an association between repair within the first 72 hours of ECMO and a shorter ECMO duration., fewer circuit issues, and a trend toward increased survival, as well as a higher chance of survival, less surgical bleeding, and a shorter ECMO stay [110–116]. In the recent study done by our team, in patients with a large CDH defect, a repair using a muscle flap or patch is possible and long-lasting, with a minimal chance of recurrence [56]. Moreover, both have statistically indifferent on-ECMO bleeding issues [54]. Surgical techniques are chosen based on the size of the defect, the patient's status, and the operator's decisions. For smaller defects, primary anastomosis is favored, whereas bigger defects necessitate an artificial patch or a muscle flap [117].

1.4.5. Outcome in CDH

In the previous few decades, advances in operational techniques, newborn care, and therapy regimens have all helped to enhance CDH management and outcomes. Although improvements increase patient survival, other factors, like the presence of thoracic liver and related abnormalities, decrease the likelihood of survival [45]. Our research previously demonstrated that when more liver tissue protruded into the chest cavity, the necessity for ECMO rose and patient survival reduced; also, this herniation lowered prenatal lung measures [45]. Another study that examined the lung-to-head ratio (LHR) and the position of the liver to determine whether isolated left CDH will survive and require ECMO found that the overall survival rates for fetuses with liver in the thorax and liver in the abdomen were 45% and 93%, respectively [92]. Infants who don't need ECMO now have overall survival rates of 70% to 90% while infants who do need ECMO now have rates of 50% [118]. Common long-term morbidities in CDH patients include recurrent respiratory infections (34%), gastroesophageal reflux (GER) (30%), failure to thrive (20%), thoracic abnormalities (40%), and cognitive impairment (up to 70%) [119–121]. A multidisciplinary team of professionals should be consulted for long-term monitoring [122]. Chronic pulmonary morbidity is typical among CDH survivors, particularly in patients who need ECMO or patch repair. Reduced forced expiratory volume in one second (FEV_1), FEV_1/forced vital capacity, forced expiratory flow at 25%–75% ($FEF_{25–75}$), functional residual capacity, and most permissible level of ventilation represent mild to moderate obstructive pulmonary disease. They also have higher bronchial hyperreactivity and lower inspiratory muscular strength [123–125]. Adolescent CDH survivors are more likely to have musculoskeletal anomalies such as scoliosis, pectus excavatum, or pectus carinatum [123,125,126]. In the long run, persistent pulmonary hypertension in the neonates (PPHN) exacerbates CDH, resulting in

considerable morbidity and mortality. Based on the progression of PAH, CDH infants can be categorized into three groups [127]. The first group has a 100% survival and no PAH. The second group had a 75% survival rate with PAH at birth that progressively goes away by the time the baby is 4-6 weeks old. The third group develops PAH that persists systemically after at least six weeks old and its mortality rate is 100% [127].

1.5. Animal models in congenital diaphragmatic hernia

Animal models for the CDH are related to the timing of the defect in the diaphragm, size, and the cause of why the lungs remain hypoplastic. The most widely used animal species are mice, rats, rabbits, and sheep. The first surgical model was performed by Lorimier and his team in the 1960s on the 72nd to 75th days of pregnancy in fetal sheep (Figure 1) [128]. The 72-75th pregnancy days are equal to the 10th weeks of pregnancy which coincide with the pseudo-glandular stage of lung development [129].

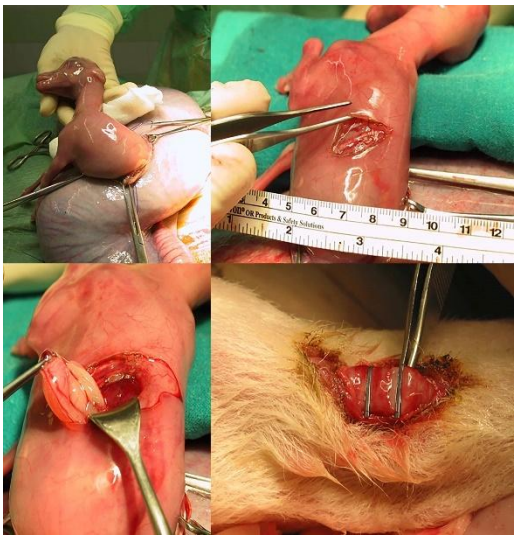

Figure 1: Creation of congenital diaphragmatic hernia with surgical technique in the sheep and tracheal occlusion with clips. (Figure was used with the permission of Prof. Jose Luis Peiró.)

Fauza et al. demonstrated the surgical CDH model on 24-25th gestational day in 1990 which was less costly, smaller in size, had a shorter pregnancy time, and a higher number of fetuses per pregnancy when compared to the sheep (Figure 2) [130]. The specified surgical models are widely used for interventional treatment methods such as tracheal occlusion, which provides lung development in utero [129,131–134].

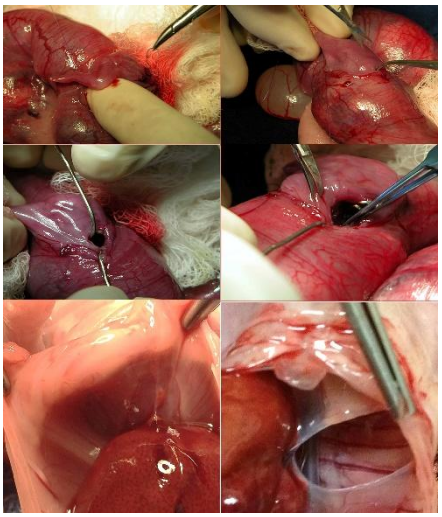

Figure 2: The surgical model to create Congenital Diaphragmatic Hernia in rabbits. (Figure was used with the permission of Prof. Jose Luis Peiró.)

Following the recognition of the carcinogenic properties of the chemical called nitrofen (2,4-dedlorophenyl-p-nitrofenl ether), a type of herbicide, it was used for toxicology studies in adult rats after which it was found to have a teratogenic effect in pregnant rats. The oral administration to the pregnant rats resulted in congenital anomalies of the lung, diaphragm, heart, and skeleton system (Figure 3) [135,136]. In this model, it has been shown that 100mg nitrofen, which is given orally to the mother as dissolved in 1mg oil on the 10th day of pregnancy, affects the development process of the lung, which begins to develop on the 11th day of pregnancy, and the diaphragm, which begins on the 13th day. While CDH occurred in approximately 70% of the fetuses, pulmonary hypertension was found in all fetuses [137]. In the same model, on the 18th day of pregnancy, occlusion of the trachea is ensured by placing 6/0 polypropylene sutures or titanium microclips into the trachea with a 2.5x binocular loop. Although this process is irreversible, its cost is very low compared to rabbit and sheep models.

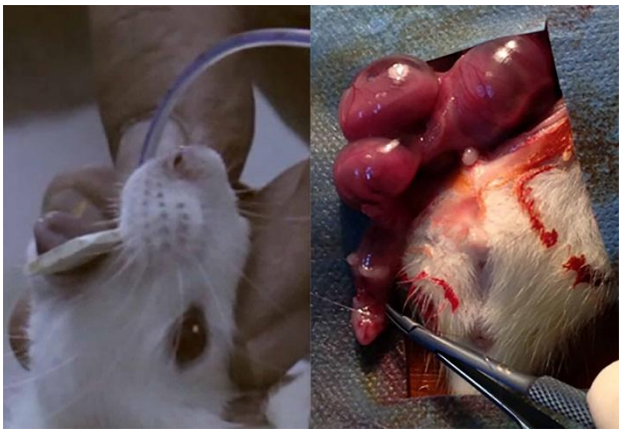

Figure 3: Oral administration of nitrofen to pregnant rats and tracheal occlusion in rat fetuses with congenital diaphragmatic hernia. (Figure was used with the permission of Prof. Jose Luis Peiró.)

The cost of the sheep model, the low number of fetuses per pregnancy, and the long gestation period are among the most important handicaps. However, it is the only model that can imitate human tracheal occlusion exactly. In the rabbit model, although the gestation period is shorter and the number of fetuses is higher than in the sheep, the fact that the model is surgical brings criticism that it does not overlap with the congenital disease model, and the size of the defect created depends on the surgeon's

preference. In the rat model, the gestation period and the number of fetuses are quite advantageous compared to sheep and rabbits. However, the chemical effect of nitrofen causes pulmonary hypertension in all fetuses, and the detection of CDH in approximately 60-70% of the fetuses causes the model to be questioned.

In the mouse model developed by Aydın et al., a new model was defined that combines the advantages of different techniques [138]. In this model, the trachea of the fetus is occluded with a suture without opening the uterine wall. One of the most important advantages of the technique is that it is reversible and allows spontaneous vaginal delivery of fetuses.

1.6. Mathematical modeling of lung structure in congenital diaphragmatic hernia

Determination of pulmonary hypertension in CDH patients and revealing lung disorders with mathematical measures enable us to better understand and detect the disease with statistics and artificial intelligence methods. In order to reveal the morphological difference between the healthy fetus's lungs and the fetus's lungs with CDH, the mathematical model of the pulmonary vascular network should be obtained.

Pulmonary capillary vessels spread in the form of a layer, while the arteries and veins have an array in the tree structure [139]. The tree-shaped sequence manifests itself in many natural structures, not only in vascular networks. For this reason, the establishment of the mathematics model of tree morphology is of interest not only to medical science but also to many different disciplines. The Strahler model is the most popular math model used for tree structures that have appeared in nature in the last 40 years. The primitive state of this model was used by Horton to model the rivers and branches and developed by the model Strahler with small changes [140,141]. Afterward, the model was used to describe various biological structures such as the retina, pial system, coronary vascular network, dendrite network in brain nerve cells, and the vascular network of the skeletal muscle in which the tree structures are seen [142–150]. Similarly, there are studies in which the lung artery and vein vascular structure are modeled by the Strahler method [151–155].

The tree structure in nature consists of branches and the root is the thickest branch, while the following branches are thinner. When modeling the tree structure, the branches are classified with different levels in terms of their distances to the root and thickness. In the Strahler model, the space separating the two branching is named as segment and the segments at the distal ends are classified as 1. Order. The number of segments increases as it progresses to the root. The branches of the schematic tree structure given in Figure 4 have been appointed according to the method of Strahler.

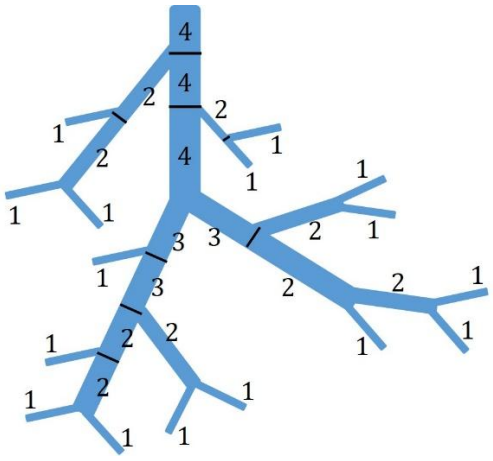

Figure 4: Order of segments according to the Strahler method

In the Strahler model, the segments are ordered according to the following algorithm from the distal ends to the root:

- The order of all distal branches is appointed as 1.
- When the two segments with the same order such as order n meet, the order of the new segment continues as n+1.
- Provided that n>m, when two segments with order n and m meet, they are appointed as order n.
- This process is continued until it is assigned to the order of the segment at the root.

When the tree in Figure 4 which was ordered per Strahler's method analyzed in detail, it will be seen that it has certain miscalculations. In a formal tree structure, branches of the same thickness are expected to be parallel to each other. However, the figure has serial connections between orders. This reduces the ability of segments to represent the branches. Another problem is although the thickness of the equal branches is the same, they are labeled in different orders. To deal with this issue, the Strahler model was modified, and the thickness of the branches and the serial connections were taken into account [156,157]. This approach, known as the diameter-defined Strahler method, ranks segments according to their diameter sizes with an iterative algorithm. The Strahler method with a defined diameter was applied to model vascular systems in various organs in humans and animals [156,158–167].

While in the traditional Strahler model, each branch is presented as order, the concept of element is defined in the diameter-defined Strahler method. The serially connected segment community of the same order is called an element. Therefore, in contrast to the standard model, branches of the same thickness defined by the element in the diameter-defined Strahler method are only parallelly connected to each other. The order of the branches defined as segments and elements in the diameter-defined Strahler method is determined according to the procedure given below:

- The order of the segments is determined according to the standard model.
- The segments of all tree structures to be modeled are pooled and then divided into classes according to their levels. The average segment diameter of each class (D_n) and the standard deviation of the diameter (Δ_n) are calculated. Assuming that the largest order is N, n = 1, 2, …, N.

- The order of all segments in the pool is updated for the following range below. To express more clearly; provided that n = 1, 2, …, N, the diameter of the segment at the n^{th} order should be in the following range.

$$\left(\frac{(D_{n-1}+\Delta_{n-1})+(D_n-\Delta_n)}{2}, \frac{(D_n+\Delta_n)+(D_{n+1}-\Delta_{n+1})}{2}\right]$$

  Herein, the left side of the range for the first order of the segments and the right side of the range for the N^{th} order of the segments could not be limited.

- The last steps are repeated iteratively until the above intervals converge. It is possible to determine the convergence criteria by looking at what percentage of the segments do not change in each iteration. For example, if 99 %of the segments have not changed, iterations are terminated.

- Provided that n = 1, 2, …, N, serially connected n^{th} order segments combine to create the n^{th} order element. Figure 5 shows the elements defined on a schematic tree.

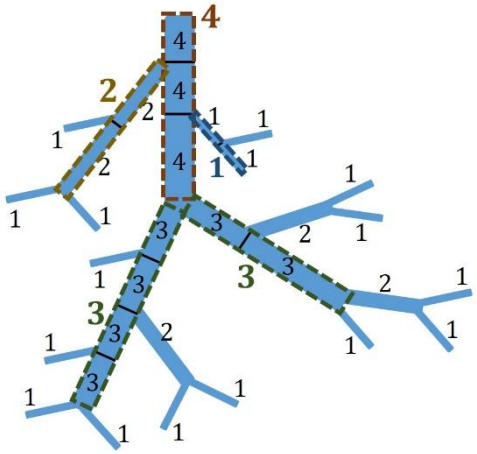

Figure 5: The elements formed by segment groups of the same order connected to the serial form are indicated by cut lines. The remaining singular segments are also defined as elements.

Once the diameter-defined Strahler method has been created, many quantitative dimensions can be defined in this model. The basic measures are the number of segments and elements for each order, their lengths, diameters, and length/diameter ratios. Apart from these simple ones, it is possible to give parameters that measure the branching behavior, branching symmetry, and fractal structure of a tree structure.

1.6.1.Segment / Element ratio

The segment/element (S/E) ratio is calculated by dividing the number of segments overall in a tree by dividing the number of segments overall elements for each order. The S/E ratio measures branching asymmetry in a tree. A value of 1 is the smallest value that the ratio can take, and this value means that branching has full symmetry. As the S/E ratio grows, the asymmetry of the branch increases. In the schematic tree given in Figure 5, the S/E ratio is approximately 1.06 for the first order, 1.25 for the second order, and 3 for the third and fourth order. Therefore, the third and fourth-order branches have higher branching asymmetry.

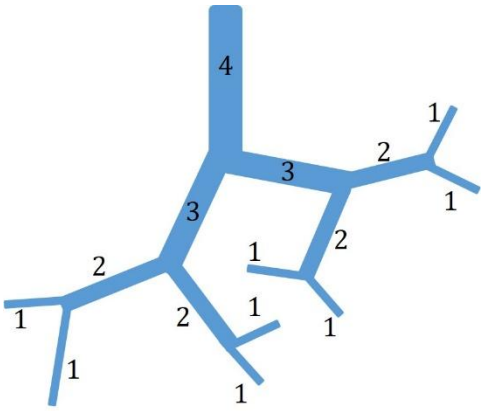

Figure 6: A tree with full branching symmetry for all levels

In the tree sample shown in Figure 6, branching has full symmetry. For this tree, the ratio of S/E is 1 at all levels. Here should be considered; The branching symmetry is not the angle or branch lengths between the branches, but that branches depend on the number of bifurcations between them.

1.6.2. Connectivity matrix

In the field of network science, understanding the complex interactions between different elements of a system is crucial. One such element is the connectivity matrix, which provides a comprehensive representation of the connections between nodes in a network. A connectivity matrix is a fundamental tool for analyzing and modeling various systems, including neural networks, social networks, and transportation networks.

A connectivity matrix, also known as an adjacency matrix, is a square matrix that represents the connections between nodes in a network. In a binary connectivity matrix, the presence or absence of a connection between two nodes is denoted by 1 or 0, respectively. However, in weighted connectivity matrices, the strength or weight of the connection is represented by numerical values. The primary goal of a connectivity matrix is to give a concise and structured representation of the connectivity patterns within a network.

Connectivity matrices have significant importance in various fields of study. In neuroscience, connectivity matrices are used to analyze and understand the functional and structural connectivity of the brain. They help identify brain regions that are strongly connected and play a crucial role in information processing. Moreover, connectivity matrices are also used in social network analysis to study patterns of interactions between individuals or groups. In transportation networks, connectivity matrices help analyze the flow of traffic and optimize routes.

The connectivity matrix of a tree describes the connection methods between different branches. Assuming that the highest order is N, the connectivity matrix is NxN square matrix, and the elements of the matrix are calculated with the following formula:

$$C_{mn} = \frac{E_{mn}}{E_n}$$

Here, E_{mn} represents the quantity of elements in the n^{th} order while E_n represents the number of elements from order n. The connection matrix for the schematic tree given in Figure 5 is given in Table 2. In trees where no branch is thickened from root to end, connection matrices are upper triangular.

Table 2: The connectivity matrix of the tree given in Figure 2

Orders	1	2	3	4
1	0/16	9/4	5/2	1/1
2	0	1/4	3/2	1/1
3	0	0	0/2	2/1
4	0	0	0	0/1

Connection matrices show the mean number of branches of the branch from each order, and this matrix can be used as an essential step in the calculation of vascular volume and blood pressure [156].

There are different methods to construct a connectivity matrix depending on the nature of the network being studied. In brain networks, connectivity matrices can be constructed using various neuroimaging techniques such as functional MRI or diffusion tensor imaging. Social network analysis often relies on survey data or online platforms to construct connectivity matrices. Transportation networks can be analyzed using data from GPS devices or traffic flow sensors.

Once a connectivity matrix is constructed, various analysis techniques can be applied to gain insights into the network's properties. One common analysis method is network centrality, which measures the importance of nodes based on their connectivity patterns. Other techniques include community detection, which identifies groups of nodes with similar connectivity patterns, and network motifs, which are recurring connectivity patterns within a network.

While connectivity matrices provide a valuable representation of network connectivity, they also have certain limitations. One limitation is the assumption of static connectivity, which may not capture the dynamic nature of some networks. Additionally, connectivity matrices may not fully capture the complexity of real-world networks due to the limitations of data collection techniques or the inherent noise in the data.

1.6.3. Fractal geometry

Fractal geometries have similar structural elements on different scales. In other words, when we look at geometry on different scales, the patterns that continuously repeat themselves are seen. This feature is called self-similarity. These fractal features are seen in the vascular tree structures of various organs [168–170]. The increase in the order of the vascular branches while the geometric increase of diameters and lengths and the geometric decrease of the number of branches is an indication of self-similarity. In cases where this fractal feature is seen, the branch diameter, length, and number comply with the Horton Law [140]. Horton Law could be defined with the below formula provided that the length, diameter, or number of the segments at the n^{th} order; a and b are fixed values.

$$\log_{10} K_n = a + bn$$

It is ideal that all branches provide the linear equation above. The degree of the above equation in a vascular tree in terms of diameter, length, and number can be considered as a measure of fractality of the tree. In practice, the average diameter, average length, or number values are analyzed separately. By calculating these parameters for each order respectively, three regression lines are determined by the

smallest frame approach. The correlation coefficients of these regression lines (R^2) become such a measure of fractality. Correlation coefficients take values between 0 and 1, and the tree is said to have more fractal properties as it approaches 1.

2. Scientific justification

Lung development is influenced by several variables, one of which is the presence of amniotic fluid. Pulmonary development is impacted by urinary system diseases that result in oligo/anhydramnios. This fact makes the egression of intrapulmonary fluid (produced naturally by the fetal lungs in development) increment and remain in less contact with the pulmonary tissue where should be for normal lung growth. On the other hand, as a result of congenital laryngeal or tracheal diseases that occlude the tracheal lumen, externally or intrinsically as Congenital High Airway Obstruction Syndrome (CHAOS), the volume and size of the lungs, as well as the growth factors that stimulate lung growth, are increased, generating pulmonary hyperplasia. Prenatal tracheal blockage as therapy was discovered as a result of this natural finding. It has the ability to improve postnatal pulmonary functioning and lung compliance by reversing hypoplastic lung [171–176].

The studies that outline an assessment of the prognosis using LHR in isolated CDH fetuses cannot be supported by other prospective investigations. The results show that, based on prenatal LHR measurement, there is no evidence of a significant relationship between lung size and postnatal course [67]. Unlike other scientists, Helling et al. were not successful in determining a predictive value for the prognosis of isolated CDH fetuses, despite the fact that the diagnosis was made between 22 and 27 weeks' gestation [67]. Furthermore, no connection was found between LHR and other postnatal breathing characteristics or the incidence of pulmonary hypertension. In this investigation, the overall survival rate was also comparable to that of other studies. The lung appears to be too complicated an organ to be prognostically evaluated only based on a single biometric measure, but still, this prenatal parameter remains the most used to estimate the severity and outcomes of these CDH patients.

Vascular nets aid in the delivery of nutrients to organs and the elimination of waste, as well as serving as a skeleton for cell and organ growth. The organization of tissues and organs relies heavily on the purposeful branching of circulatory systems. Even if these branching techniques differ slightly between individuals, cellular cues that trigger vascular development in disease situations have a significant impact on them [177]. Many acquired or congenital disorders that alter pulmonary vascular modeling have been reported in the literature, including emphysema, CDH, and bilateral renal agenesis [178]. It is critical to be able to distinguish the difference in vascularity in diseased ones using a simple and repeatable method, as well as to reveal and classify its properties in both experimental investigations and human situations. Although histological examination of tissues retains its historical importance, radiological methods have begun to be used in experimental studies because histological methods have too many staining procedures, the samples lose their compliance with different technical evaluations, and it is difficult to reveal the entire lung tree in detail. With today's technological capabilities, histological tissue diagnosis is the only known way to diagnose PAH in utero in human samples. In the case of CDH, however, a biopsy is not regarded as a diagnostic procedure because one of the lungs does not develop adequately, and the other lung, while partially developed, is anatomically and functionally problematic. Furthermore, the biopsy material's diagnostic accuracy in predicting the overall lung state is unknown. Intelligent radiological techniques have become increasingly important at this stage. Many researchers are working hard today to use radiological technologies to reveal the pulmonary vascular tree [133,179,180]. It is a subject that has been studied for many years, and these studies may be presented in the most precise way by using artificial intelligence algorithms to eliminate human mistakes.

Mice, rats, rabbits, and ovine models are used to demonstrate the pathogenesis of the disease and to establish appropriate treatment choices [28,134,136,181]. Because of the large number of fetuses

in every pregnancy, the rat model is preferred. The ovine model, on the other hand, is the most human-like. While tracheal occlusion in other laboratory animals is accomplished by placing a metal clip or stitching outside of the trachea, in the ovine model, an inflating balloon can be introduced into the trachea for occlusion in the same way that it is done in humans [173]. In the ovine model, the balloon is also removed to allow newly created intrapulmonary fluid to wash away the thicker mucus coating in the lungs after a prolonged period of occlusion, allowing the lungs to be compliant for spontaneous or aided ventilation following birth. This surgery, known as unplug, is critical for postpartum survival. Other animal models, except for ovine, hinder the translation of studies into humans because tracheal occlusion was not reversible in them. However, our recent model enables us to study the outcomes of unplug procedure in the mice [134,182].

The current physiopathology of CDH causes lung development to be disrupted, as well as airway and vascular branching. In pulmonary arteries, this action causes not only numerical scarcity but also an increase in the thickness of the existing channel wall structure. Because of the reduced blood flow in the lungs during pregnancy, blood pressure (the pressure applied to the artery wall surface) does not rise. In the postnatal period, however, the pressure on the surface rises with the commencement of respiration and an increase in the amount of blood moving through the lung vessels. Unfortunately, this condition, known as PAH in the postnatal period, cannot be assessed accurately in the prenatal period. The segmentation of lung vascular networks in adults is done using radiological diagnostic tools and software, primarily computerized tomography (CT). All these products, however, demand user interaction. This intervention wastes time and labor and may result in bias. It is critical to have systems that do not require user participation and run automatically. In research using radiological methods in animal models to highlight vascular architecture, materials such as plaster, silicone, and other materials have been employed. Because the chemicals used in these approaches are administered intravenously at a constant pressure, they may cause the vessels to rupture or alter their relationships in the three-dimensional plane. As an alternative to these agents, a water-soluble iodine-based contrast agent (Lugol) was used, which was diffused homogeneously in the intravascular area of the rat fetus, and the numbers of vessels, diameters, lengths, and angular relationships with each other in the 3-dimensional plane were revealed using commercially available software, Analyze.

In fetuses with CDH, gastrointestinal organs protrude into the thorax causing hypoplasia of the lung parenchyma and vasculature, which generates substantial morbidity and mortality in infants. Significant PAH-related mortality and morbidity are linked to anatomical changes in the pulmonary vasculature. There is a critical need to prenatally evaluate and treat PAH before these patients need to use the lungs to improve their survival. Some fetuses with CDH have undergone fetal surgery for TO, which prevents the egress of intrapulmonary fluid, and seems to expand the lungs, remodeling vasculature, and improving survival and postnatal lung function. Any developing structure in the embryonic or fetal body follows the vasculature pattern so makes sense that the well-described decrease of branching in the airways of CDH hypoplastic lungs also will have defective branching on the lung vasculature.

3. Hypotheses

Since pulmonary hypertension is one of the predictors of the survival of these patients, this thesis study seeks to test the general hypothesis that a newly designed prenatal pulmonary vascular branching index correlates with the severity of postnatal pulmonary hypertension.

4. Objectives

Main Objective

To elucidate the morphological distinctions in fetal pulmonary vasculature between normal and congenital diaphragmatic hernia (CDH) subjects through μCT imaging.

Secondary Objectives

1. To demonstrate the normal three-dimensional distribution, branching patterns, and interrelations of pulmonary vasculature in animal models using μCT scans, providing a baseline for normal lung anatomy.
2. To quantify and compare the morphometric properties of the pulmonary vasculature in CDH-affected fetuses, focusing on variations in lung and lobe vasculature, branching frequency, alveolarization, compliance, and the thickness of the pulmonary arterioles' muscular layer.
3. To demonstrate the anatomical and morphological disparities in pulmonary vasculature through detailed μCT scan analysis, thereby facilitating the understanding of CDH's impact on lung development; and to develop a radiologically based index capable of distinguishing between healthy and CDH-affected pulmonary anatomy, enhancing diagnostic accuracy and potentially guiding therapeutic interventions.

5. Materials and methods

5.1. Study design

This is an experimental prospective study (Figure 7). The National Institutes of Health's Guide for the Care and Use of Laboratory Animals was followed in all experiments after receiving ethics committee permission (NIH Publications No. 80023, revised 1978). Approval of IRB #2017-6361 and IACUC #2016-0111 by the Cincinnati Children's Research Foundation Institutional Animal Care and Use Committee, #2018.234.IRB1.027, #2018.236.IRB1.029 and #2018.HADYEK.027 by Koç University Institutional Animal Care and Use Committee and by #3E-46048792-050.01.04-19244 Tekirdağ Namik Kemal University Institutional Animal Care and Use Committee were granted. All surgical procedures were performed while the mother was under isoflurane inhalation general anesthesia. The fetal anesthesia for intrauterine management was also well delivered through this. Following the puppies' carbon dioxide euthanasia, all procedures on the newborn were carried out.

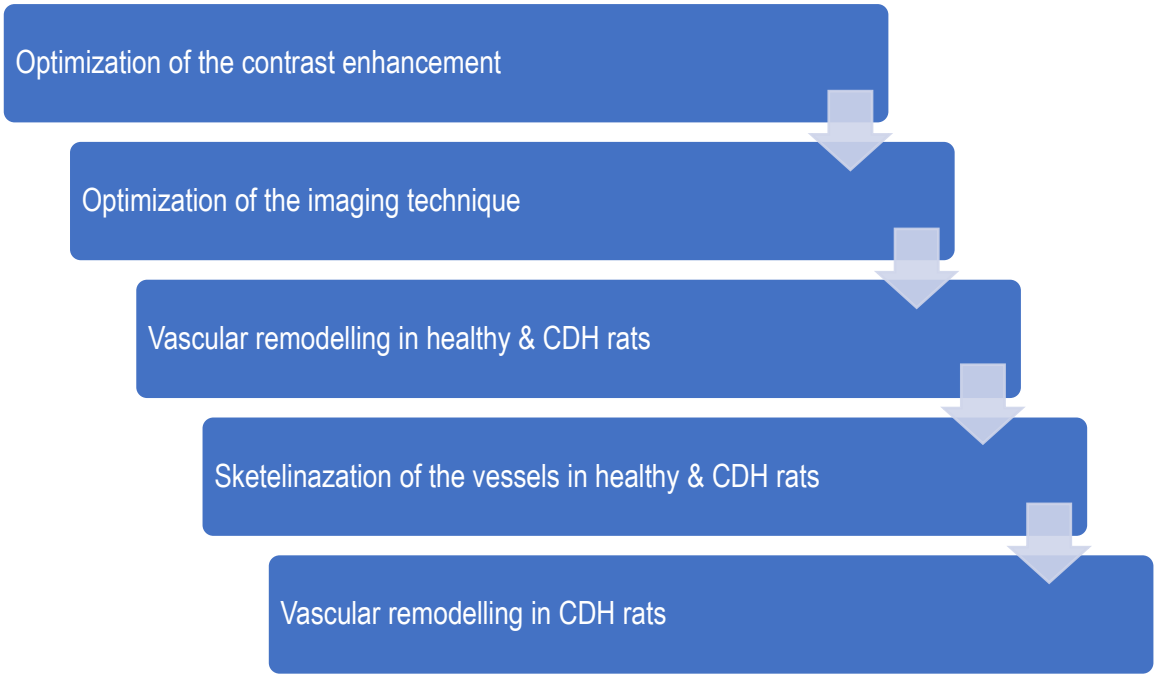

Figure 7: The flow chart of the study

5.2. Creation of CDH

Age-matched Sprague Dawley rats were mated overnight, and the females' plugging, and weight increase were scaled daily. The first day of the pregnancy was regarded to be the day on which sperm were found in a vaginal smear. On the ninth embryonic day (ED), 100mg of nitrofen (2,4-dichloro-4'-nitrodiphenyl ether), a teratogen herbicide, was gavaged into the pregnant rats with olive oil to cause a congenital diaphragmatic hernia. The control group received no intervention.

5.3. Preparation of the fetuses

At ED 21 (full gestational length of 22 days), cesarean sections were used to deliver the fetuses. The puppies were gently dried and placed on a cool pad. Umbilical cords were promptly tied to stop blood loss because red blood cells are required for intravascular Lugol binding. Carbon dioxide was used to euthanize fetuses.

5.4. Specimen preparation

As an intravascular contrast agent, Lugol solution (10g KI and 5g I_2 in 100 ml H_2O) was employed (Figure 8). It was made into a physiologically isotonic solution by diluting it with de-ionized water to improve diffusion and lessen soft tissue shrinking [183]. Phosphate-buffered saline and 4% paraformaldehyde (PFA) were used to fix fetuses overnight (PBS). For 72 hours, they received treatment with a 25% Lugol solution. In order to represent the comparison of the pulmonary tree, four more distant vascular branches from various specimen groups — the isolated lung, the upper half of the torso, the direct right ventricle injection (injection group), and the whole body with partial excision of the thoracic skin (2mm in diameter)—were prepared. The main defense against Lugol perfusion is the skin. To evaluate iodine's absorption through the pulmonary vessels and identify the preparation that produced the best Lugol penetration, four rats were analyzed in each group.

Figure 8: The administration of the Lugol solution

5.5. Micro-CT imaging

A MicroCAT II micro-CT scanner was used in this study (ImTek, Inc., Knoxville, TN). The useable field of view for the scanner geometry used in this case was about 3x2 cm. The following parameters were used to capture raw data during the course of a 55-minute scan: 80 kVp, 200 A, 800 projections, 0.25° increment, 3.3 s exposure, and 2-by-2 binning of the CCD detector's 3072 x 2048 element array. Feldkamp cone beam filtered back projection was used to reconstruct the projection data after it had been adjusted for distortion and detector anomalies. As a result, a 3D image with an isotropic resolution was produced of 21 m and a voxel size of 19 m.

5.6. Image analysis

Data was collected, and an image of the pulmonary arterial tree in 3D was made utilizing the commercial program Analyze 12.0 (Rochester, MN). The pulmonary vascular tree was reconstructed in three dimensions over a number of steps. After manually choosing the area of interest, a segmentation per threshold was then tailored for the specimen. On the stained vasculature, seeds — which are one of the pixels in the desired area — were chosen, and the object was extracted using the "region grow" function. The 'object separator' function, which the user can manually set, and the vessels that weren't part of the pulmonary system were excluded. A 3D volume rendering method was used to create the

detailed 3D representations of the vascular tree. Using the "generate tree" function, tree analysis—i.e., measurement of the pulmonary vessels' diameter and length—was carried out [184,185]. Lastly, the software automatically determines the number of branches and generations.

5.7. Data acquisition

All fetuses were harvested at E21 (full gestation is 22 days) by cesarean section under general anesthesia. μCT was performed after intravascular contrast introduction and images were analyzed by Analyze Pro (Rochester, MN, USA) [133]. After excluding the low contrast and abnormal data due to technical error of the machine, 11 right and 10 left arterial trees of the healthy rat fetuses, and 10 right and 10 left arterial trees of the rat fetuses with left CDH were included in this study.

5.8. Data processing

5.8.1. Segmentation

Unnecessary areas of the CT pictures were clipped to save time and effort. Analyze Pro used image processing techniques. After manually defining the appropriate threshold, the photos were subjected to a semi-automated tracking technique for region growth. The seed placement on the vessel points was tracked by the region-growing algorithm, which built the vessel structures. This method can be employed when the vessel distributions' pixel values are clearly different from those of other tissues. The region expanded could not monitor the entire network in some situations due to the contrast agent's distortion. To solve this problem, the threshold value was configured to be very little., which resulted in network structure noise. The segmentation process by hand removed the noise. Both arteries and veins were covered by the segmented construction. They were manually separated and the data for pulmonary arteries were included in this study.

5.8.2. Nomenclature

The skeletonization process was applied utilizing multiple thinning algorithms to extract bifurcation patterns and morphometric measurements such as number, the mean cross-sectional area, and the length of vessels [186]. This process also classified vessels according to their generations. Per this classification a segment is defined as the part of a vessel between two bifurcation nodes that follow each other in a tree structure; an element is defined as a set of segments that are connected in series and have the same order and an order is defined as the branch or generation in a tree structure.

5.8.3. Mapping of the tree structure

In a formal tree structure, Order 1 was assigned to the roots of arterial trees and the ordering number was increased as the generations increased. This ordering scheme did not take the diameter or cross-sectional area of vessels into account. Therefore, for a more effective ordering scheme, Strahler's approach was modified in a way to consider the cross-sectional area of vessels [187]. This modification was similar to the approaches that considered the diameter of vessels in an iterative manner [157,165]. This modified approach classified the smallest cross-sectional area vessels as order 1, and the order number of vessels increased along with their cross-sectional area. The modified approach that was applied individually for the right and left sides of arterial trees consisted of the following steps:

i) The arterial trees were modeled as a Strahler system [188]. In this system, between two succeeding nodes of bifurcation on a vessel was called a 'segment'. The orders of these segments increased from leaves to the root, however, they were not determined according to their cross-sectional area.

ii) An iterative procedure was applied to the obtained model to rearrange the orders of segments according to the cross-sectional area. This iterative procedure was similar to the one that was applied according to the diameter of segments [157,165].
iii) The order of a segment was increased if it was lower than the order of the next generation.
iv) The elements, which were groups of segments joined in series in the same order, were determined [157,165]. The vessel segments defined the serial features of the arterial trees, while the elements defined the parallel features.
v) The iterative procedure in the second step was applied to the elements.
vi) If the elements of the same order were connected in series, they were merged and labeled as a single element.

For some arterial trees, the preceding generations might have had thinner thickness due to failures in the imaging or skeletonization processes. In such cases, the modified Strahler's approach would produce unrealistic arterial tree models [157,165]. Step (i<ii) in the algorithm was included to eliminate such failures. Thus, the proposed approach considered the generation orders as well as the thickness of the vessels.

5.8.4. Connectivity matrix

Finally, the connectivity matrix for each arterial tree was computed to describe the links between vessels of various orders [157]. An element in row m and column n of the connectivity matrix, namely C_{mn}, was defined as the ratio of the total number of elements of order m springing from elements of order n to the total number of elements of order n. The elements C_{mn} of connectivity matrices were filled with zeroes for $n < m$ since only the elements for $n \geq m$ were meaningful in Strahler's system. Moreover, if the accompanying artery tree lacked an element of order n, the value of an element C_{mn} was taken to be 0.

5.9. Histological analysis

All samples were histologically analyzed and compared to verify the distinctions and the diagnosis. Following the euthanasia of the fetuses, the fetal weight was measured first, followed by the CT scan, and then complete excision of the lung tissues and bronchial tree, followed by the measurement of the lung weight. The tissues were placed in liquid nitrogen after their weight had been determined and stored there until a tissue examination. RNA PCR, Western-Blot, and immunohistochemistry were performed on the obtained samples.

5.9.1. Hematoxylin & Eosin staining

For histological examination, H&E was used, and samples were perfused with 10% formaldehyde solution at 20cmH_2O pressure for 1 hour and then kept in 10% formaldehyde solution at 4°C for 24 hours. The tissues were then paraffinized, the lung tissues were sliced 5µm thick and examined with H&E to reveal the staging of lung development with the Zeiss Axio Scope A1 light microscope.

5.9.2. Mason Goldner (Trichrome) staining

Selective viewing of erythrocytes, vascular components, and connective tissue is possible with Masson-Goldner (Trichrome) staining. The chosen tissue sections in this staining protocol were cut into 5µm thick sections, embedded in paraffin, and stained with Weigert's iron hematoxylin first. Second, to produce trichromic staining, tissues were stained with azophloxin solution, tungstophosphoric acid orange G solution, and light green SF solution, respectively and the Zeiss Axioscope A1 light microscope was used to see the sections.

5.9.3. Immunofluorescence and Western Blot analysis

Factor VIII (von Willebrand Factor), CD34, CD31, collagen type 4, and smooth muscle alpha-actin levels were measured in the tissue to indicate the presence of pulmonary hypertension.

Factor VIII (von Willebrand Factor) is an important blood clotting protein. It was found that the amount of von Willebrand factor is high when pulmonary hypertension and congenital heart disease are present in patients [189,190]. Its amount was also found to be increased in cases of pulmonary hypertension [191].

CD34 is a marker of vascular endothelial precursor cells, embryonic fibroblasts, and hematopoietic stem cells. It has been used to demonstrate vascular endothelium in studies of rats with congenital diaphragmatic hernia and rats with pulmonary hypertension [192,193]. In the case of pulmonary hypertension, bone marrow-derived proangiogenic precursors are found to be elevated [194].

A marker of endothelial cells is CD31, also known as platelet endothelial cell adhesion molecule also takes an active role in the formation of new vessels [195]. It was used as an endothelial cell marker in a study on the contribution of endothelial to mesenchymal transition to endothelial dysfunction in pulmonary arterial hypertension [196].

Collagen type 4 is the main collagen component of the basement membrane and is important for basement membrane stability. It was shown that endothelial dysfunction, which is one of the main features of the pathogenesis of pulmonary arterial hypertension, is decreased [197]. It has increased in proportion to the severity of the disease in cases of pulmonary hypertension [198].

Vascular smooth muscle cells include smooth muscle alpha-actin that provides support for vascular motility and contraction. Vascular remodeling in pulmonary arterial hypertension involves the accumulation of mesenchymal-like cells that synthesize smooth muscle alpha-actin, so smooth muscle alpha-actin is important for demonstrating the presence of pulmonary hypertension [199]. However, it was found to be increased in the proximal vessels in cases of pulmonary hypertension [200].

Immunohistochemistry and western blot procedures were performed using the above-mentioned cell markers. For the immunohistochemistry procedure, first of all, lung tissues were fixed in 10% neutralized formalin, after necessary dehydration, clearing, and infiltration steps, they were embedded in paraffin and using a microtome, paraffin-embedded tissues were divided into 5 m slices. Immunohistochemistry staining was performed using the Mouse and Rabbit Specific HRP-DAB Detection IHC Kit (AB64264, Abcam). After rehydration of the tissues, slides were boiled in citrate solution for antigen retrieval, followed by proceeding in accordance with the protocol of the commercial kit. The cell markers mentioned above were used as primary antibodies in this process and the secondary antibody was provided by the kit. After counterstaining with hematoxylin, dehydration steps were followed, and the slides were sealed with Entellan™. Imaging of the slides was done with the Zeiss Axio Scope A1 light microscope. Analysis of the images to be obtained will be done using the Fiji biological image analysis program, with a focus on assessing differences in staining intensity between groups.

The lung tissues that stored at -80^0 were used primarily for protein isolation for the western blot procedure. After adding protein extraction solution and protease inhibitors to these tissues to prevent protein degradation, the tissues were homogenized and sonicated, followed by the supernatants formed at the end of the centrifugation. BCA analysis was performed with a microplate reader to obtain amounts of supernatants and protein and the values obtained were used for western blot. The isolated protein

samples were mixed and incubated with the loading solution prepared with 2-mercaptoethanol and 4x Laemmli sample buffer solution, and then loaded onto the Mini-PROTEAN TGX gel (Bio-Rad) placed in the Mini PROTEAN Tetra system tank (1658004EDU, Bio-Rad) with the protein marker. and the required running solution, Tris-Glycine-SDS buffer solution, filled the tank. The gel was run at 95 V for approximately 1-2 hours, with regular control. A PVDF membrane (Bio-Rad) was used for the gel-to-membrane transfer step, and after the transfer cassette was formed, it was placed in the tank, the tank was filled with the transfer solution and run at 40° to 40 V overnight to allow the transfer to take place. After the necessary blocking and washing steps, the primary antibody was applied to the membrane overnight, and then the secondary antibody was applied for an hour. Finally, imaging was performed using the Chemidoc XRS+ (Bio-Rad) instrument to provide chemiluminescent signal detection with the Pierce ECL Western Blot Substrate kit (32106, Thermo Scientific). The analysis of the obtained gel images was done using the Fiji biological image analysis program, focusing on protein concentration calculations and intergroup comparisons on the images.

5.10. Statistical analysis

The statistical analysis was performed using IBM SPSS Statistics 20.0.0 (Chicago, IL). The mean and standard deviation are used to express data. The distribution's normality was demonstrated via the Kolmogorov-Smirnov test. The variables' homogeneity was analyzed using a one-way ANOVA. Student's T-test and Pearson correlation were used for parametric data. If the p-value was 0.05, statistical associations were deemed significant. The mathematical calculations for the measures including the number, length, cross-sectional area of segments and elements, segments/elements (S/E) ratio, length/diameter (L/D) ratio, and connectivity matrix, and their statistical analysis were conducted in MATLAB (MathWorks Inc., Natick, MA). The data were expressed as mean ± standard deviation. For the above-mentioned measures excluding the connectivity matrix, the differences between the right and left lungs as well as the lungs with and without CDH were analyzed by using a two-sided Mann-Whitney U test. Mann-Whitney U test was also used to investigate the statistical differences between each corresponding element of the connectivity matrices, whereas the overall difference between connectivity matrices was analyzed through the analysis of similarities (ANOSIM) test [201]. The threshold for statistical significance was set at p 0.05.

To avoid bias in the statistical tests, the cross-sectional area-based Strahler's approach was applied for the pooled data of both sick and healthy rat fetuses, and the ordering schemes were determined individually for their left and right lungs. Correspondingly, the segments and elements were assigned orders between 1 and 4. The cross-sectional area-based ordering scheme was specified according to the means given in Table 3.

Table 3: Intervals for the ordering scheme

Orders (n)	**1**	**2**	**3**	**4**
Intervals for Left Lungs (μm)	17.34	45.30	66.73	119.02
Intervals for Right Lungs (μm)	14.15	38.75	63.03	138.72

6. Results

6.1. Gross results

There were 70 fetuses examined throughout the study, 40 of which were used in the first part to demonstrate the feasibility of the Lugol application while the rest were used in the second part. In the latter one, 15 (50%) of the fetuses had CDH while the other half served as the control. To increase the effectiveness of penetration of the pulmonary tree by the iodine stain, various iodine introduction techniques were tested such as direct injection, extracted lung, whole body without any intervention, half body (upper half), and partial skin removal. Lugol diffused uniformly throughout the capillaries in the pups with partially removed skin, allowing fine-grained imaging of the lung vasculature (Figure 9). This way this method becomes the best choice.

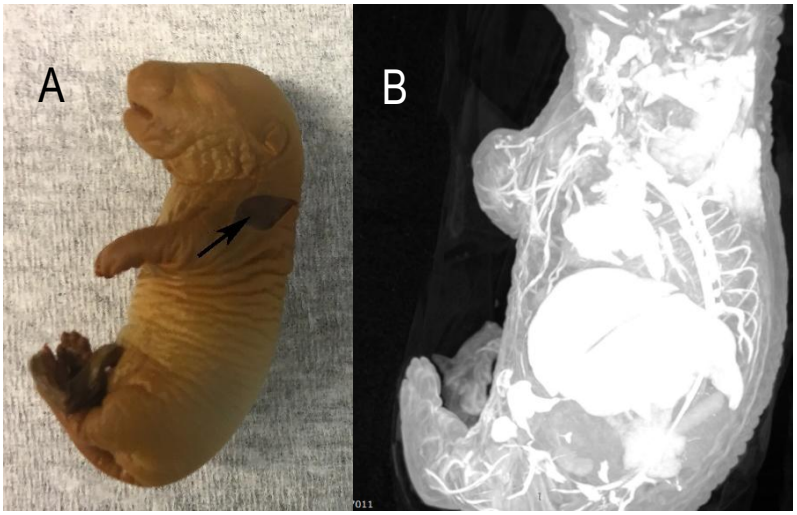

Figure 9: A: Partially peeled skin of a rat fetus (arrow), B: Contrast enhancement of the fetus under micro-CT.

On the other hand, a CT scan revealed no visible arteries in an isolated entire lung from a fixed fetus that had been exposed to Lugol solution (Figure 10). Moreover, the contrast agent directly given to the right ventricle was an unexpected failure, with little to no apparent vasculature and a considerable amount of contrast agent pooling in the heart. This might be due to the loss of blood from the injection side. Due to severe blood loss, although the fetal body was submerged in the Lugol solution, the iodine stain barely partially penetrated, making it impossible to see the entire pulmonary tree.

Figure 10: Embryos' micro-CT scans. A: The right ventricle is immediately injected with contrast material. B: The fetus' upper half of its body is immersed in Lugol solution. C: The skin is partially peeled off in option.

6.2. Visualization of fetal lung microvasculature

For each group, eight rat fetuses were scanned to enhance the model for displaying the lung vasculature (Figure 11). The method of partially excised skin, which caused very little blood loss, was the only strategy that worked that allowed observation of each sample's microarchitecture.

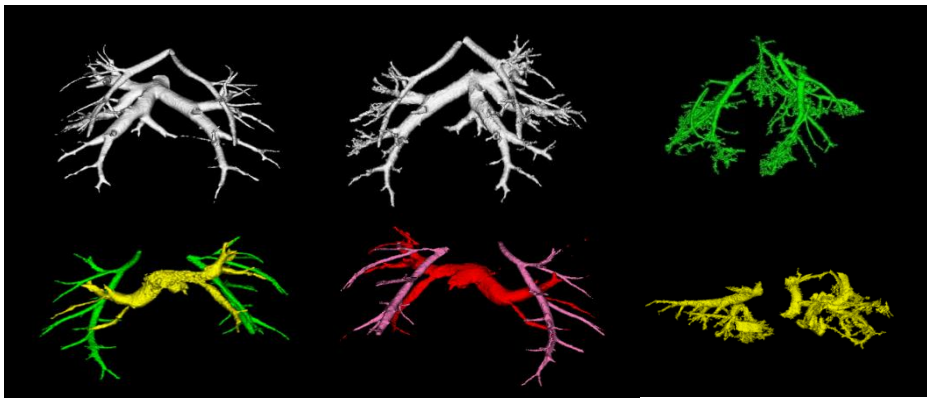

Figure 11: The vascular structures gathered through different Lugol applications.

To minimize the blood loss, the body of the fetus was cooled on a cold pad, and the umbilical cord was clamped immediately after birth, prior to skin incision. This method demonstrated the 3D interconnectedness of the entire fetal lung as well as the high-generation arteries' side branches. Iodine stained just the blood, and bleeding in puppies prevented the entire pulmonary vascular tree from filling until the level of the alveolar capillaries, making it impossible to see the pulmonary microcirculation clearly. On embryonic day E21 of a rat fetus, the micro-CT data collected and processed by the software revealed all vasculature dispersed throughout the lung (Figure 12). The pulmonary vascular tree served as a model for the configuration and architecture of the lungs.

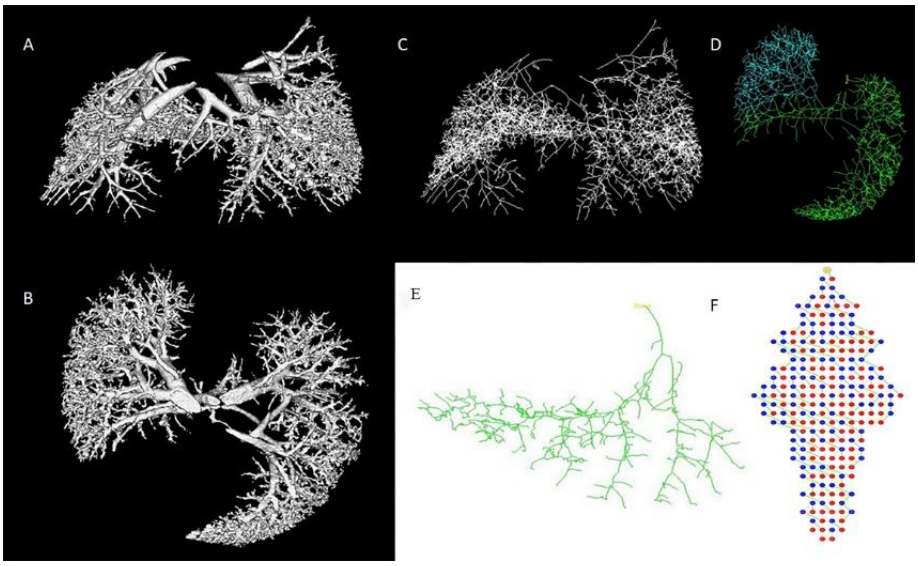

Figure 12: A partial skin specimen that underwent ex vivo Lugol treatment produced three-dimensional images of the whole lung vasculature in the coronal and axial planes (A, B), the whole pulmonary vascular system being reduced to a skeleton (C), analysis of a single lobe's vasculature using a colored picture (D), and skeleton of vascular network in the right lobe (E) with mapping, which aids in measuring all vessel parameters by either choosing the junctions between the vessels (blue [mid-branches] and red [end branches]), or the vessels themselves (yellow and green) (F).

After skeletonized tree structures were available, the vessels' branch generation information and number of branches were discovered. The root point of the tree structure was manually assigned at the beginning of the artery. Once the root point selection was complete, the initial location when the tree structure deviates from normal was given a new node (Figure 13).

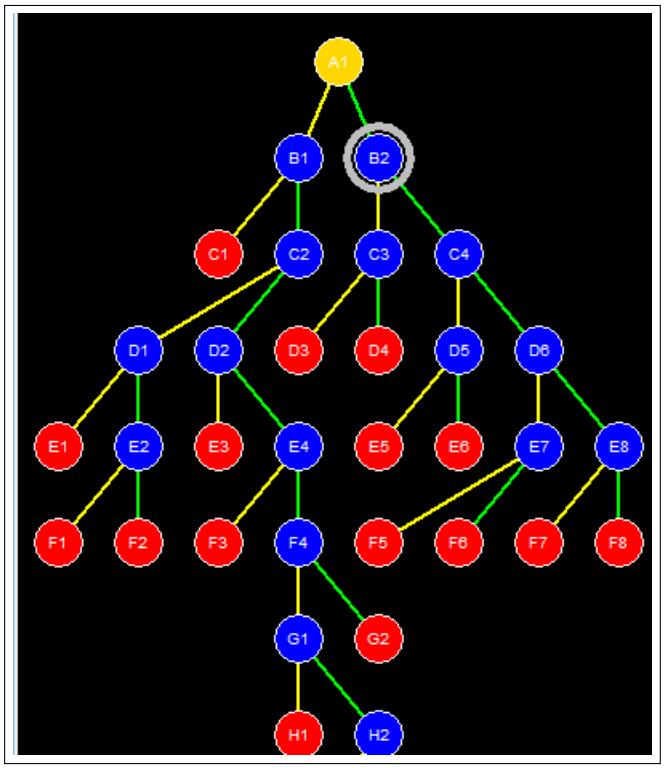

Figure 13: Mapping of the tree structure

Binary structures and skeletonized structures were rendered to determine the area of the branches (Figure 14).

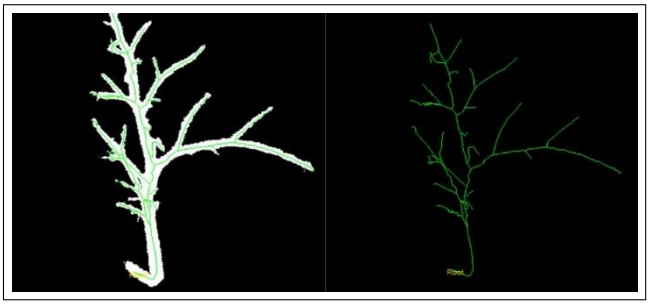

Figure 14: Rendered view of the tree structure of the lung vasculature.

Then, measurements of the tree structure were taken, and a radius value was computed for each node. Each output from the tree structure was recorded into a file for the later part of the study (Figure 15).

Name	Area Product	BAP St Dev	Average Area	Area St Dev	Length	Children (Name,Angle)	
A1	0.00	0.00	101.25	4.86	4	(B1, 142.6)	(B2, 27.0)
B1	0.00	0.00	135.47	21.04	94	(C1, 131.8)	(C2, 160.8)
C1	0.00	0.00	108.14	18.71	22	(D1, 170.0)	(D2, 103.7)
D1	0.00	0.00	47.71	21.50	28	(E1, 133.3)	(E2, 130.3)
E1	0.00	0.00	28.90	10.95	10		
E2	0.00	0.00	29.02	14.39	44		
D2	0.00	0.00	72.54	20.12	24	(E3, 151.7)	(E4, 92.3)
E3	0.00	0.00	47.33	7.73	15	(F1, 119.8)	(F2, 159.0)
F1	0.00	0.00	15.47	17.23	32		
F2	0.00	0.00	42.24	7.25	54	(G1, 142.2)	(G2, 154.7)
G1	0.00	0.00	27.62	24.79	13		
G2	0.00	0.00	22.69	12.98	39		
E4	0.00	0.00	16.81	31.67	26		
C2	0.00	0.00	144.90	3.40	21	(D3, 108.6)	(D4, 166.0)
D3	0.00	0.00	121.17	19.27	18	(E5, 124.2)	(E6, 172.0)
E5	0.00	0.00	71.57	44.93	14		
E6	0.00	0.00	140.20	4.14	15	(F3, 168.5)	(F4, 114.6)
F3	0.00	0.00	57.24	31.18	51	(G3, 105.9)	(G4, 171.5)
G3	0.00	0.00	33.12	16.05	60		

Figure 15: An example of a tree structure analysis

Two distinct methods were used to compare artery architecture. Using the first method, the vasculature of both lobes was compared. Figure 12 displays the measures of the vessels' length, cross-sectional area, and branch count. The alternative procedure, which was more thorough, involved ranking the right and left arteries by the size of their cross-sections and comparing those rankings for each lobe separately. When the root point was chosen to serve as the artery's entry point, Analyze™ automatically allocates the node points generations higher. However, because the widths of the vessels were neglected when generations were ordered in this manner, comparisons might not produce accurate results. Arranging the rat artery branches per the dimensions of their cross-sectional areas, a modified Strahler's stream order approach was employed. The tributaries of the river are arranged in the stream order system of Strahler based on their magnitude. A higher-order branch results from the union of two identical orders, but when two different orders combine, the larger branch receives the degree. The area between the two bifurcations in the diameter-defined Strahler system is referred to as a segment. Elements are formed by combining segments in the same sequence that are serially aligned. Figure 16's bottom right corner shows the combination of two orders and two branches, however, due to the fact that this approach also takes diameters into account, the resulting generation is still order two rather than order three.

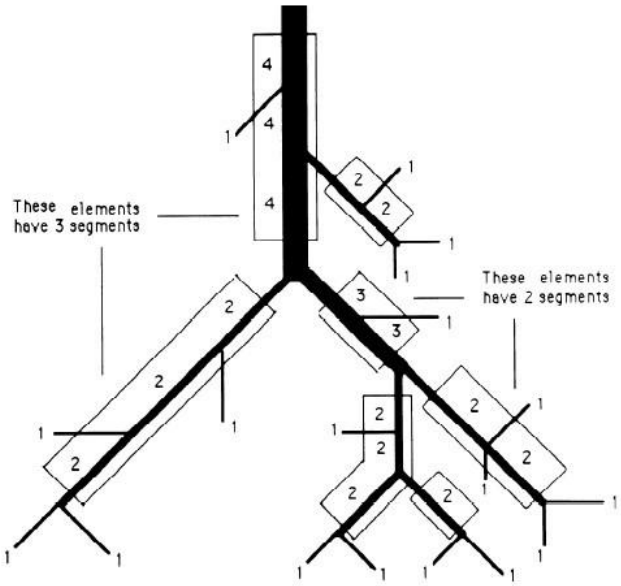

Figure 16: Strahler system with defined diameter [157].

6.3. Morphometry

Our morphometric results were subjected to the modified Strahler method, and four orders were established based on cross-sectional area values (Figure 17).

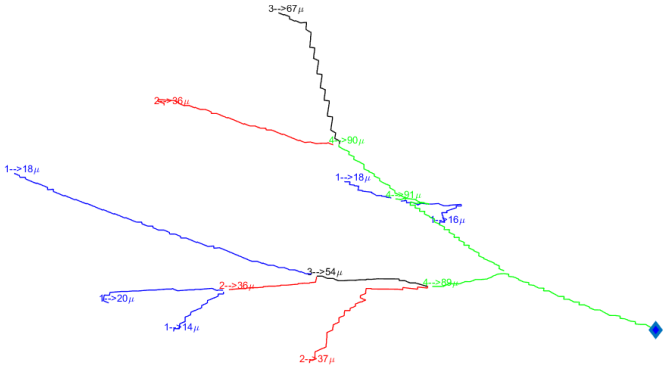

Figure 17: An illustration of branches of an organized artery

The pulmonary tree's mean number of segmented vessels was 900 ± 24 (mean ± SD), and their average diameter was 134.13 ± 53.00µm (range 40.72-265.69µm). Table 4 summarizes the measures of the arteries and veins in comparison. Although vessels could be divided into arteries and veins up to the 30th generation, most branches belonged to the 11th through 30th generations (Figure 18). There was no statistically significant difference between the number of arteries and veins in the same lung ($p>0.005$).

	RPA	RPV	LPA	LPV
Area of vessel (µm²)	36.38 ± 28.86	52.46 ± 42.01	40.64 ± 28.03	47.01 ± 39.16
Vessel length (µm)	21.02 ± 14.31	20.64 ± 14.4	19.3 ± 13.04	22.26 ± 13.51
Diameter of the vessel (µm)	122.97 ± 46.07	145.78 ± 60.18	131.14 ± 45.46	137.68 ± 57.72
Circumference of the vessel (µm)	386.32 ± 144.75	457.98 ± 189.05	411.97 ± 142.82	432.53 ± 181.34
L/D ratio	0.20 ± 0.15	0.18 ± 0.14	0.18 ± 0.14	0.21 ± 0.16

Table 4: The morphometric results per vessel type. (RPA: Right pulmonary artery, RPV: Right pulmonary

vein, LPA: Left pulmonary artery, LPV: Left pulmonary vein, L/D ratio: Vessel length to diameter ratio.) (Values expressed as means ± standard deviations)

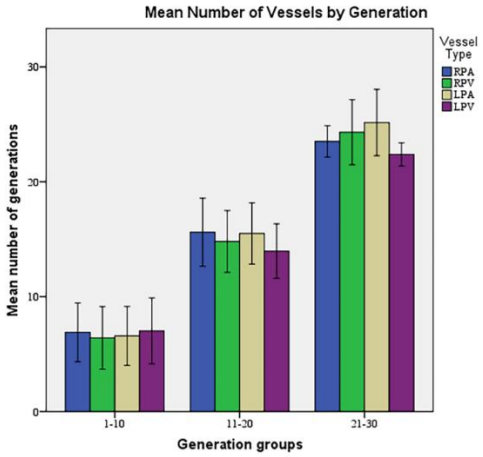

Figure 18: The average number of vessels for each type of vessel over generation groups. (RPA: Right pulmonary artery, RPV: Right pulmonary vein, LPA: Left pulmonary artery, LPV: Left pulmonary vein.)

6.4. Histology

6.4.1.Hematoxylin and Eosin staining

To assess the developmental variations in the lung tissues obtained from fetuses in the control and nitrofen groups at ED21, H&E staining was performed. H&E staining of fetal lungs from ED21 showed dilated airspaces in the control group (Figure 19). However, in the nitrofen-exposed fetuses, even though their lungs seemed to have a close dilation to the control group, the alveolar airspaces were not thinned enough, and the cellular linings were much more compact.

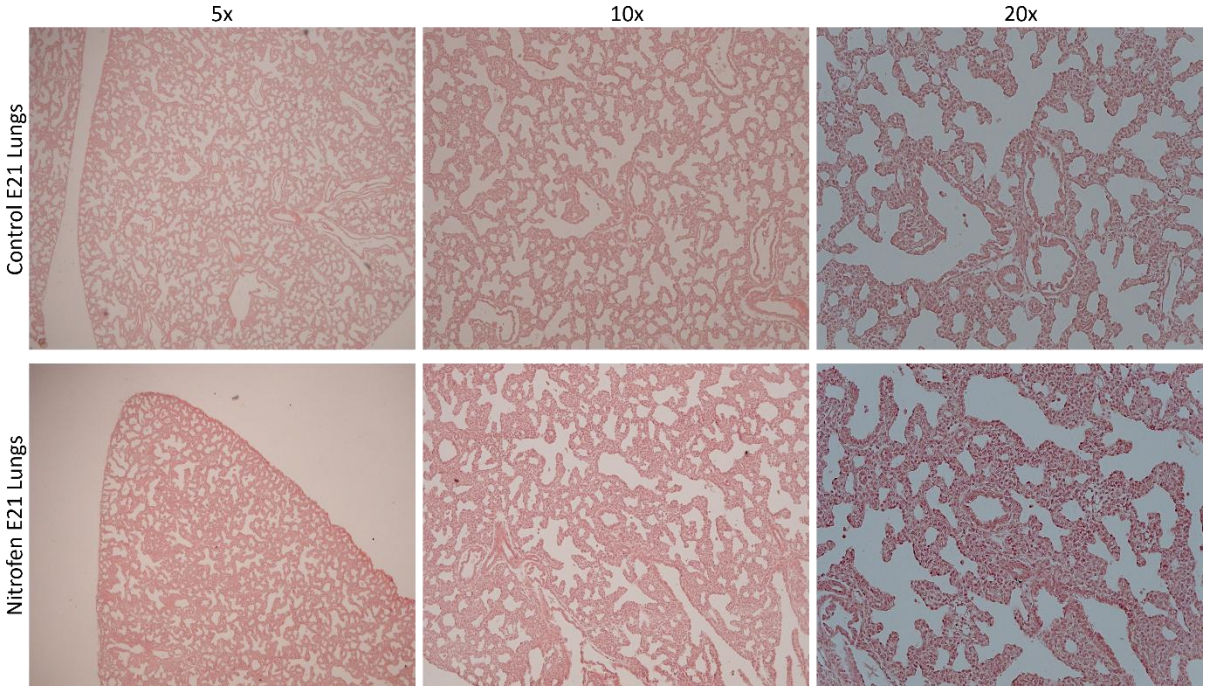

Figure 19: Hematoxylin and eosin staining of lungs from control and nitrofen-exposed fetuses at ED21.

6.4.2.Masson-Goldner staining

For selective visualization of the pulmonary vasculature, Masson-Goldner staining was performed. Similar to H&E staining, Masson-Goldner staining of lung tissues from the control fetuses at ED21 showed more dilated airways compared to nitrofen-exposed lungs (Figure 20). However, staining did not allow pulmonary vasculature to be distinguishable in the control group. In the images obtained from the nitrofen-exposed lungs, sections showed a more intense reddish color, possibly due to less developed airway dilation and more cellular compactness. Even though pulmonary vessels surrounded by connective tissue can be seen with the green-blue colored elements, pulmonary vasculature was not distinguishable enough to acquire a comparison between the groups.

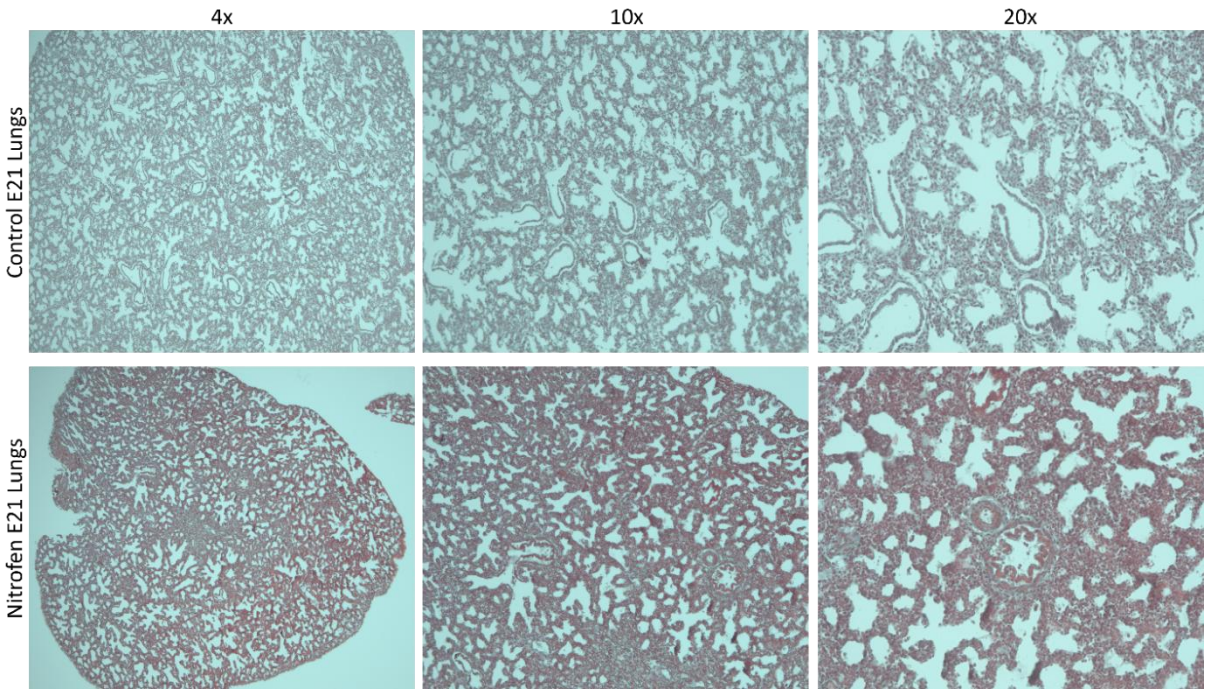

Figure 20: Masson-Goldner staining of lungs from control and nitrofen-exposed fetuses at ED21.

6.4.3.Immunofluorescence staining

To demonstrate the presence of PAH in the lung tissues obtained from the nitrofen-exposed fetuses and compare them to the control group, the lung tissues were stained with primary antibodies against alpha-smooth muscle actin (α-SMA) and von Willebrand factor (vWF) with an immunofluorescent approach.

Immunofluorescence staining of α-SMA showed specific and robust expression both in vascular smooth muscle cells (vSMCs) surrounding pulmonary vessels and in airway smooth muscle cells (aSMCs), which enclose the bronchioles (Figure 21).

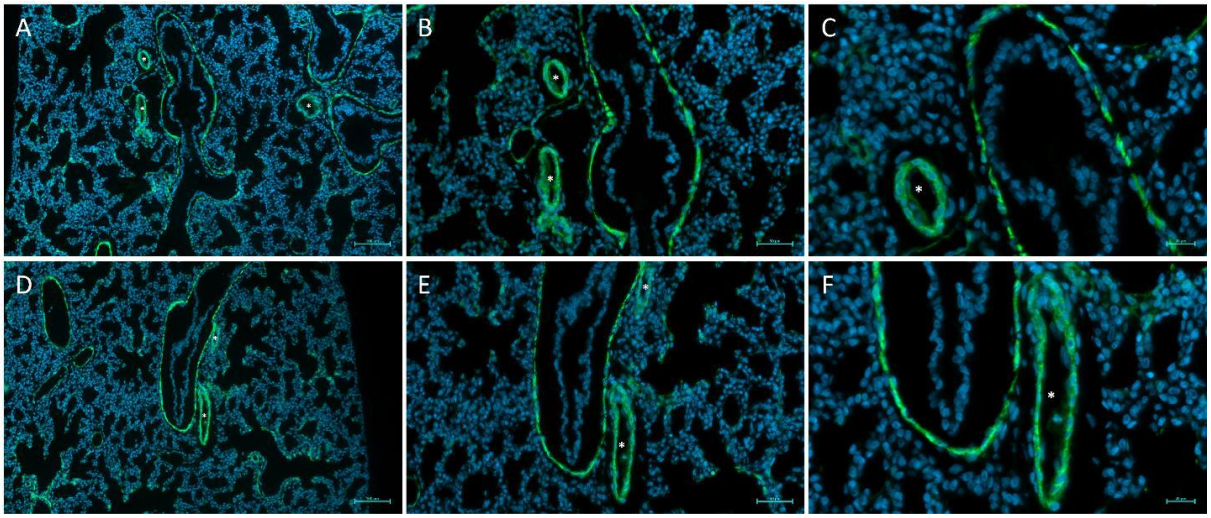

Figure 21: Immunofluorescence staining of lung tissue from the control group at ED21 for alpha-smooth muscle actin (α-SMA). α-SMA staining was strongly seen in vascular smooth muscle cells (vSMCs, asterisks) surrounding pulmonary vessels and airway smooth muscle cells (aSMCs) surrounding bronchioles.

Immunofluorescence staining of vWF showed strong expression in regions that are considered to be vascular endothelial cells (Figure 22).

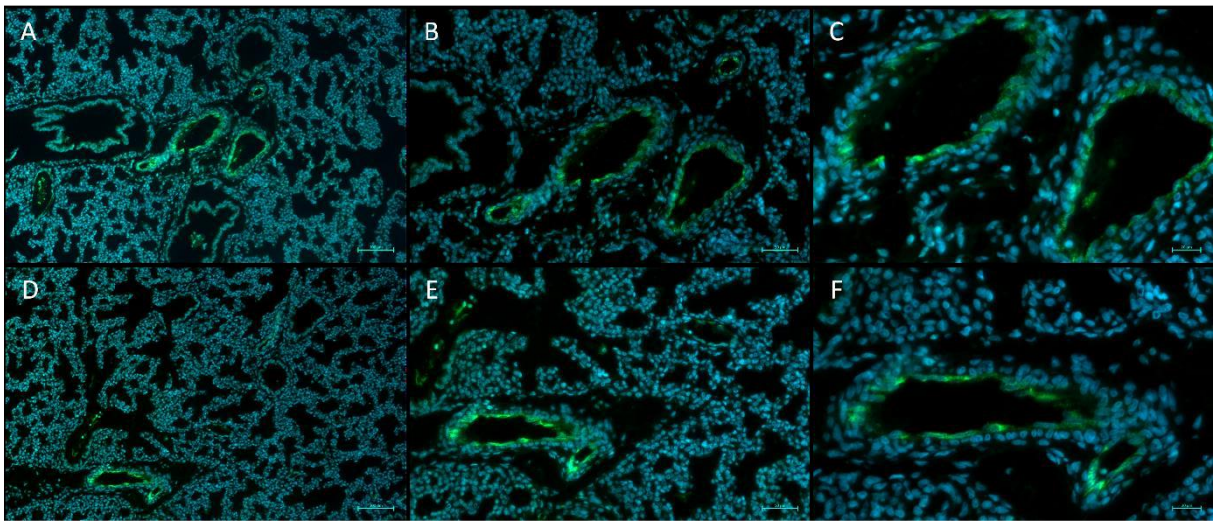

Figure 22: Immunofluorescence staining of lung tissue from the control group at E21 for von Willebrand factor (vWF).

6.4.4.Western Blotting

For the assessment of α-SMA and vWF protein expression levels, western blot was performed both in control and nitrofen-exposed fetal lungs at ED21 with 60 µg and 40 µg as alternatives for optimization. To ensure equal protein loading amounts, β-tubulin was used as a loading control. Even though the membrane containing the β-tubulin protein lane was not properly cut, it showed almost similar expression in the samples loaded as 60 µgs (Figure 23). However, vWF showed no expression in both control and nitrofen groups in 60 µgs which might be due to the high protein amount present and because

of the high molecular mass of vWF. vWF gave slight expression in both groups, but it was not quantifiable enough for assessment.

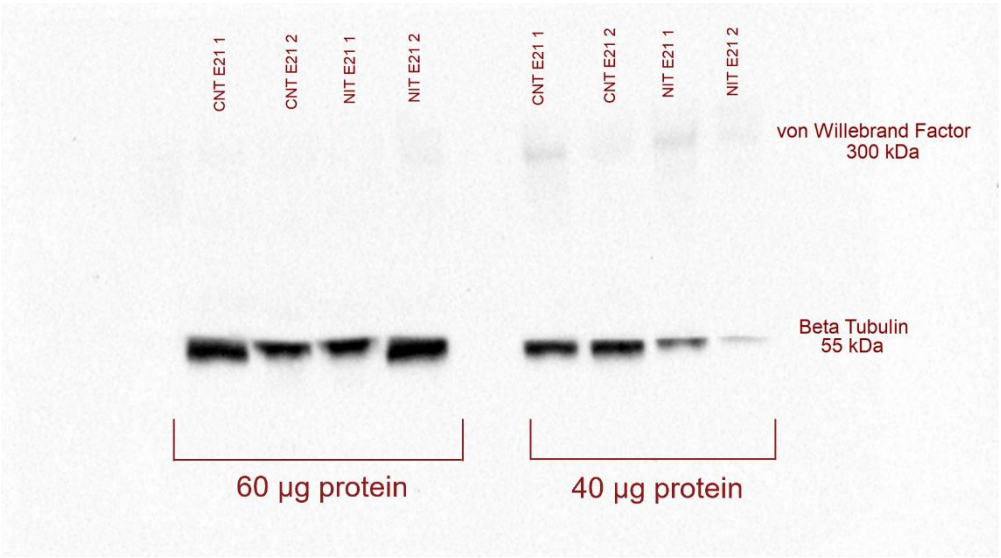

Figure 23: Protein expression levels of vWF and β-tubulin in loaded amounts of 60 µg and 40 µg of protein from lungs of control and nitrofen-exposed fetuses at ED21.

Improper cutting of the membrane exposed to α-SMA primary antibody did not allow proper assessment for both control and nitrofen-exposed fetal lungs (Figure 24).

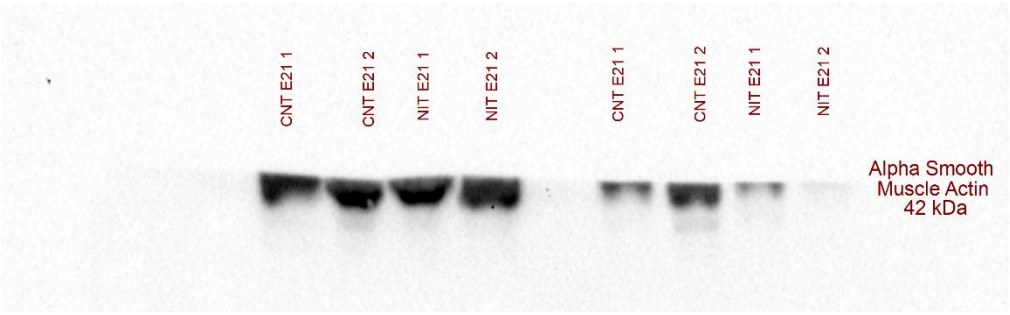

Figure 24: Protein expression levels of α-SMA in loaded amounts of 60 µg and 40 µg of protein from lungs of control and nitrofen-exposed fetuses at ED21.

6.5. Group comparison

There were 30 fetuses analyzed with CT, of which 15 (50%) were controls and 15 (50%) were rat fetuses with CDH. To analyze the diseased and normal subjects, the right and left lungs were examined separately (Figure 25). When compared to the intact diaphragm in the normal group, the defects in the left diaphragm of the nitrofen-induced CDH group were type D per CDH Study Group Staging, and in all cases, a combination of the large and small bowels, stomach, spleen, and liver herniated into the chest.

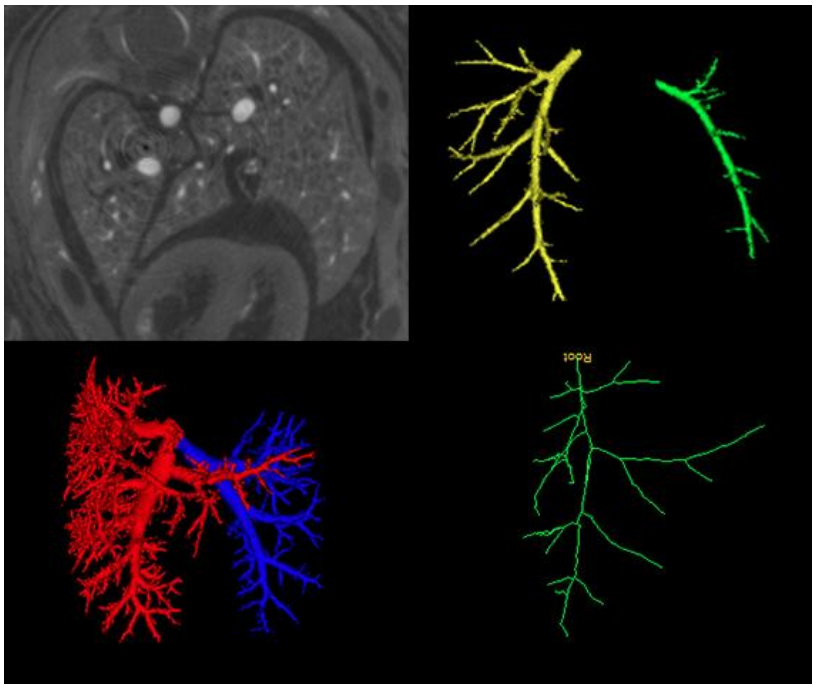

Figure 25: A: Micro-CT scan of the fetal lung, B: Segmentation of the arterial vasculature, C: Segmentation of the venous vasculature, D: Skeletonized Right Artery

6.5.1. Comparison of total networks

Table 5 compares the morphometric results for the networks of rat arteries. The parameters of the CDH groups and the control group's left and right lobes were evaluated separately. At the left lobe, there was no discernible difference in the mean (std) value of the vessels' cross-sectional area between healthy and sick subjects (p=0.43), but at the right lobe, it was smaller in the control group (p=0.015). For both lobes, there were no statistically significant variations between the vessel lengths of both groups. For both the left and right lobes, there were fewer branches in sick participants compared to control subjects (P 0.05).

Table 5: Comparison of the lung morphometry

	Left			Right		
	Control	CDH	p	Control	CDH	p
Cross-Sectional Area	57.09 ± 18.95	71.05 ± 15.53	0.431	56.83 ± 17.81	92.16 ± 26.75	**0.015**
Vessel Length	32.02 ± 6.17	40.42 ± 13.84	0.817	35.32 ± 3.57	30.05 ± 9.56	0.727
Number of Branches	30.78 ± 13.15	14.20 ± 7.44	**0.029**	42.20 ± 12.19	15.40 ± 6.62	**0.002**

6.6. Results of tree structure mapping

Table 6 shows the total number of pooled segments and elements for each order of the lungs in healthy and CDH fetuses. When compared to the control group, the CDH group had a significantly smaller number of segments and elements, notably in the distal vasculature.

Table 6: The numbers of pooled segments and pooled elements

n	Pooled Segment Numbers				Pooled Element Numbers			
	Left		Right		Left		Right	
	Control	CDH	Control	CDH	Control	CDH	Control	CDH
1	118	11	123	0	95	11	105	0
2	62	17	133	20	49	15	99	19
3	52	24	111	18	30	13	70	12
4	77	20	101	31	15	6	24	12

For order 1, CDH had fewer segments than the control group on both the left (U=2.5, p=0.004) and right (U=0, p=0.001) sides (U=0, p=0.001), while there was no difference for order 4 as expected, there was a significant difference for orders 2 and 3 solely on the right side (U=1 (p=0.001) and U=6 (p=0.012), respectively (Table 6). In the control group, there were also more segments in the right lung than the left lung, but only for orders 2 and 3 (U=13, p=0.003, and U=16.5, p=0.007).

Table 7: Comparison of the mean number of segments and elements

n		Left			Right			Left -Right*
		Control	CDH	U, p	Control	CDH	U, p	U, p
Segments	1	11.80 ± 7.57	2.20 ± 2.28	**2.5, 0.004**	11.18 ± 6.82	0.00 ± 0.00	**0, 0.001**	52.5, 0.888
	2	6.20 ± 3.36	3.40 ± 0.89	9.5, 0.062	12.09 ± 3.75	4.00 ± 2.55	**1, 0.001**	**13, 0.003**
	3	5.20 ± 4.21	4.80 ± 4.09	23, 0.855	10.09 ± 5.24	3.60 ± 3.05	**6, 0.012**	**16.5, 0.007**
	4	7.70 ± 4.90	4.00 ± 4.06	15.5, 0.264	9.18 ± 4.92	6.20 ± 2.59	13.5, 0.120	45.5, 0.529
Elements	1	9.50 ± 5.34	2.20 ± 2.28	**4, 0.005**	9.55 ± 4.97	0.00 ± 0.00	**0, 0.001**	53, 0.916
	2	4.90 ± 3.21	3.00 ± 1.00	15, 0.237	9.00 ± 3.44	3.80 ± 2.28	**3.5, 0.005**	**20, 0.015**
	3	3.00 ± 2.26	2.60 ± 1.67	25, 1.000	6.36 ± 3.64	2.40 ± 1.95	9.5**, 0.042**	**24, 0.031**
	4	1.50 ± 0.97	1.20 ±0.84	20, 0.638	2.18 ±1.25	2.40 ±0.55	24, 0.718	38, 0.223

*Control group

The statistical analysis that was performed for the number of elements yielded similar results (Table 7). There were differences only between the elements of small orders in both left lungs (U=4 (p=0.005) for elements of order 1) and right lungs (U=0 (p=0.001) and U=3.5 (p=0.005) for elements of orders 1 and 2) of subjects with and without CDH. The number of elements in the right and left sides of healthy lungs for orders 2 and 3 were significantly different (U=20, p=0.015, and U=24, p=0.031).

Table 8: Comparison of the mean length of segments and elements

n		Left			Right			Left -Right*
		Control	CDH	U, p	Control	CDH	U, p	U, p
Segments	1	40.74 ± 18.85	34.59 ± 21.42	521.5, 0.284	44.80 ± 27.75	-	-	6966, 0.592
	2	43.36 ± 25.09	55.14 ± 59.36	521, 0.948	48.18 ± 37.25	43.75 ± 29.04	1268.5, 0.741	4100, 0.949
	3	30.76 ± 26.41	30.47 ± 22.17	611.5, 0.893	41.83 ± 37.93	52.20 ± 36.57	775, 0.129	2417, 0.097
	4	32.22 ± 34.41	36.09 ± 42.48	752.5, 0.880	33.36 ± 25.31	33.34 ± 24.37	1559, 0.974	3472.5, 0.226
Elements	1	50.61 ± 27.23	34.59 ± 21.42	343.5, 0.064	52.48 ± 31.90	-	-	4945, 0.920
	2	54.86 ± 40.79	62.49 ± 68.34	345, 0.727	64.72 ± 49.95	46.06 ± 29.72	724.5,0.115	2197, 0.355
	3	53.31 ± 69.73	56.26 ± 53.40	168, 0.483	66.34 ± 60.23	78.30 ± 50.20	309.5, 0.149	878, 0.197
	4	165.40 ± 109.11	120.29 ± 113.67	33, 0.371	140.41 ± 107.87	86.14 ± 63.13	109, 0.247	153, 0.444

*Control group

The lengths of segments and elements were pooled for each order of the subject groups and were analyzed similarly for the differences between the left and right lungs and the control versus CDH

lungs. Although the CDH group has a lower number of elements and segments both on the right and left side compared to the control group none revealed any statistically significant differences (Table 8).

Figure 26 illustrates the fitted lines using a least squares algorithm. Horton's Law was observed in the control group's pooled element numbers (R^2=0.996 for left lungs, R^2=0.811 for right lungs), while the CDH group violated this regulation (R^2=0.395 for left lungs, R^2=0.750 for right lungs). Although a high R^2 was found for element numbers of the right lung of rats with CDH, the linear relationship would be disrupted if the element numbers of order 1 were included in the analysis. These results indicated that CDH not only decreased the number of elements of small orders but also destructed the fractal structure of the pulmonary arterial trees regarding the number of elements. Since the pulmonary arterial trees of rat fetuses were not mature yet, the elements were not long relative to the roots (elements of order 4). Therefore, the pulmonary arterial trees of the rat fetuses did not sufficiently obey Horton's Law (R^2=0.635 for left lungs, R^2=0.795 for right lungs). Moreover, this issue prevented the interpretation of the effect of CDH on the fractal structure regarding the element lengths. On the other hand, the modified Strahler's approach applied here considered the cross-sectional area of vessels for the pooled data of both CDH and healthy rat fetuses. The diameters in all groups obeyed the Horton's Law (R^2=0.991 for the left lung of the control group; R^2=0.992 for the right lung of the control group; R^2=0.979 for the left lung of CDH group and right lung of CDH group R^2=0.998).

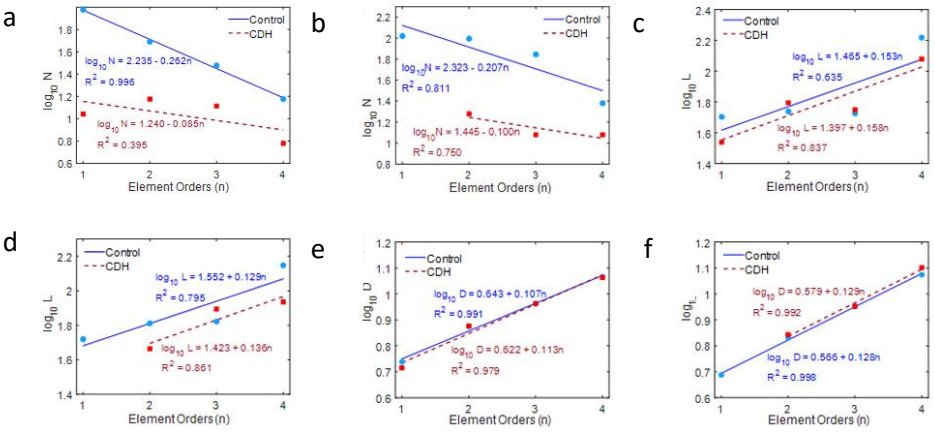

Figure 26: The link between the quantity of pooled elements and the order numbers for the left (A) and right (B) lungs, the length of pooled elements, and the order numbers for the left (C) and right (D) lungs, the diameter of pooled elements and the order numbers for the left (E) and right (F) lungs.

The mean segment/element (S/E) ratio accounts for the degree of asymmetry of ramification. The S/E ratio was highest for order 4, which meant that the vessels of this order had the highest asymmetry of ramifications (Table 9). The statistically significant difference was only on the left side for order 1 (U=4, p=0.010) and on the right side for order 2 (U=8.5, p=0.028). When the ratio of the length to the diameter of the vessels (L/D) was analyzed, the only difference was found between the healthy and CDH fetuses on the right side for order 2 (U=7, p=0.019).

Table 9: Comparison of the mean S/E and L/D ratios

n		Left			Right			Left -Right*
		Control	CDH	U, p	Control	CDH	U, p	U, p
The Mean S/E ratio	1	1.20 ± 0.16	1.00 ± 0.00	**4, 0.010**	1.13 ± 0.15	-	-	38.5, 0.251
	2	1.58 ± 1.30	1.20 ± 0.45	21, 0.634	1.46 ± 0.64	1.04 ± 0.08	**8.5, 0.028**	42, 0.370
	3	2.09 ± 1.74	1.71 ± 0.64	24.5, 0.996	2.10 ± 1.55	1.57 ± 0.42	22, 0.565	42, 0.358
	4	5.96 ± 3.76	3.00 ± 1.63	16.5, 0.330	4.44 ± 1.76	2.53 ± 0.70	10.5, 0.055	49.5, 0.724
The Mean L/D Ratio	1	8.80 ± 1.94	6.90 ± 2.77	11, 0.099	10.23 ± 2.92	-	-	36.5, 0.218
	2	7.68 ± 3.59	9.25 ± 5.82	19, 0.514	10.34 ± 4.69	6.49 ± 2.53	**7, 0.019**	29, 0.073
	3	6.96 ± 6.33	5.58 ± 2.43	23.5, 0.886	9.64 ± 6.98	9.59 ± 3.30	26, 0.913	32, 0.113
	4	16.36 ± 9.58	10.38 ± 7.17	21, 0.679	12.07 ± 5.02	7.08 ± 3.03	15, 0.180	53, 0.916

*Control group. S/E stands for segment/element ratio; L/D stands for length/diameter ratio.

6.7. Results of connectivity matrix

Table 10 shows the mean of the connectivity matrices that belonged to the vessels in the left and right lungs of healthy and CDH fetuses. Connectivity matrices represent the average branching number of elements of each order. For example, element C_12 of the matrix given for the left lungs of the control group denotes that the average number of elements of order 1 springing from the elements of order 2 is 0.76 with a standard deviation of 1.52. Since it is unrealistic to have thick vessels springing from thin vessels in an arterial tree, connectivity matrices are upper triangle matrices. On both sides of healthy arterial trees, the average number of elements of order 2 and 3 springing from the elements of order 4 (C_24 and C_34) was higher than the average number of springing elements of other orders. This quantitative relation was also preserved for the CDH fetuses within their own groups. On the other hand, when comparing with healthy fetuses, these averages mostly decreased especially for the springing elements of order 1.

Table 10: Comparison of the mean of connectivity matrices

Orders		Control				CDH			
		1	2	3	4	1	2	3	4
Left lung	1	0.19 ± 0.15	0.76 ± 1.52	1.49 ± 1.90	1.18 ± 1.31	0	0.10 ± 0.22	0.37 ± 0.65	0.40 ± 0.55
	2	0	0.05 ± 0.13	0.50 ± 0.49	1.62 ± 1.56	0	0.10 ± 0.22	0.38 ± 0.36	0.70 ± 0.67
	3	0	0	0.06 ± 0.16	1.82 ± 2.15	0	0	0.15 ± 0.22	1.30 ± 1.10
	4	0	0	0	0.32 ± 0.28	0	0	0	0.20 ± 0.27
Right lung	1	0.11 ± 0.15	0.39 ± 0.59	1.07 ± 0.78	0.33 ± 0.40	0	0	0	0
	2	0	0.07 ± 0.08	1.12 ± 1.32	1.45 ± 0.81	0	0.03 ± 0.07	0.53 ± 0.51	0.77 ± 0.72
	3	0	0	0.10 ± 0.17	2.42 ± 1.41	0	0	0	1.00 ± 0.94
	4	0	0	0	0.44 ± 0.30	0	0	0	0.57 ± 0.09

There was a statistically significant difference between the C_{11} elements of the left lungs (U=5, p=0.014) as well as the C_{13} of the right lungs (U=2.5, p=0.003) of the subjects with and without CDH (Table 11). These differences belong to the average number of elements of order 1 springing from the elements of order 1 in the left lungs of the control and CDH groups, and the average number of elements of order 1 springing from the elements of order 3 in the right lungs of the control and CDH group. The connectivity matrix could be considered as a single measure that describes the average number of connections of elements of different orders with each other. Accordingly, to investigate the differences in the entire connection scheme, an ANOSIM test was applied by using the Euclidean distance of matrices. As a result, the null hypothesis that the similarity between groups was equal to the similarity within the groups was

accepted (R=0.127, p=0.191 for the right lungs with and without CDH, R=-0.150, p=0.876 for the left lungs with and without CDH and R=0.075, p=0.058 for healthy left and right lungs).

Table 11: U, p values for connectivity matrices

Orders	**Control – CDH (Left)**			
	1	***2***	***3***	***4***
1	**5, 0.014**	15.5, 0.270	13.5, 0.167	15, 0.227
2		24, 0.813	23.5, 0.886	16.5, 0.360
3			19.5, 0.484	23, 0.842
4				19, 0.690
	Control – CDH (Right)			
	1	***2***	***3***	***4***
1	15, 0.212	10, 0.058	**2.5, 0.003**	12.5, 0.115
2		19, 0.346	22, 0.558	15, 0.166
3			17.5, 0.362	10.5, 0.054
4				24, 0.731
	Left – Right (Control)			
	1	***2***	***3***	***4***
1	36, 0.180	52.5, 0.885	51, 0.805	30, 0.078
2		38, 0.183	28.5, 0.066	53.5, 0.943
3			46, 0.453	33, 0.127
4				39, 0.245

7. Discussion

Despite advancements in disease management, congenital diaphragmatic hernia still has a high mortality and morbidity rates among babies. The researchers have put a lot of work into using prenatal diagnostic methods to determine prognostic factors to predict the severity and postnatal survival. To extrapolate the degree of pulmonary hypoplasia, antenatal imaging is mostly focused on measurements of lung area or volume. Pulmonary hypertension should be categorized prenatally to improve accuracy in predicting the severity of the disease, but nowadays no measurable antenatal factor seems appropriate. The current prognostic parameters are based on the correlation of prenatal and postnatal markers in retrospective patient data [45]. In the development of the embryo and fetus, the lung vasculature is especially important since the main concern is the development and arborization of the lung from the bronchial and vascular point of view. As a result, fetal lung vascular modeling applications have received a lot of attention. Understanding the fetal pulmonary tree and its quantitative analysis is critical for predicting the severity of the hypoplasia and understanding the etiology of PAH in congenital diaphragmatic hernia.

The approach for visualizing the fetal lung vasculature has already been proven [133]. In order to enable the homogenous passive diffusion of the intravascular contrast material, various techniques were utilized. Additional distal vascular branches from four different specimen groups were prepared to compare the visualization of the pulmonary tree. These specimen groups included an isolated lung, the upper half of the torso, a direct right ventricle injection (injection group), and a whole body with partial thoracic skin excision (2mm in diameter), as the skin is the main barrier preventing Lugol perfusion. To evaluate the iodine's diffusion into the pulmonary vasculature and ascertain which preparation produced the best Lugol penetration, four fetuses from each group were scanned individually. The isolated lung did not work due to excess loss of blood during the isolation process. Inserting the upper half of the torso into the Lugol solution resulted in the same outcome due to loss of blood. The direct injection of Lugol into the right ventricle enabled the passive diffusion of the contrast, however, the blood loss through the entrance point of the injector resulted in a heterogenous distribution of Lugol. The partial removal of the skin while the whole body is preserved resulted in the best characterization of the vasculature. On the other hand, the visibility of the lungs was considerably impaired in CDH fetuses due to the abdominal organs herniating into the thoracic cavity. Because the fetuses were not alive and there was no blood flow, the procedure did not apply pressure to deliver the contrast material into the intravascular area, which may have led to some squeezed arteries being missed. Although the Lugol solution was passively diffused into the vascular region, since these vessels may have been constricted, causing the CT scanner to miss them. The fetuses were immediately utilized after birth to avoid bias in this comparison.

Many different biological systems' structure and function have been modeled using networks and network theory. Systems that span scales from cells to ecosystems include metabolic processes, food webs, host-parasite webs, disease dynamics, gene regulatory networks, and social interactions. As a result, structural archetypes such as themes, scale-free behavior, modularity, the presence of hubs, and small-world structures have been identified. These theories, however, frequently do not consider the spatial limitations that govern the positions and connections of nodes and edges. There are several types of supply and distribution networks, where the nodes and edges are actual physical entities interwoven in space, including leaf venation networks, cardiovascular networks, cortical networks, root networks, ant trails, and road networks. Since physical restrictions have a significant impact on how biological networks are organized, theory is also necessary to describe these networks.

Even though the idea of spatial networks is rather varied, it frequently makes certain simplifications when it is applied to biological resource delivery networks. An example of a perfectly self-similar structure is a network, such as a splitting binary tree, under the fractal branching theory. The cardiovascular system is thought to be a fractal with physical properties that have evolved to efficiently transport fluid from the aorta to capillaries, according to a popular idea of metabolic scaling in mammals. Similar presumptions are made using this model to analyze the above-ground organization of tree branches. With a growing understanding that the initial fractal branching assumption is overly straightforward, both models have sparked a wide range of follow-up research. For instance, biological physical networks are not completely balanced binary trees but rather feature side branches. The study of river networks is where the first theories of side-branching resource distribution and delivery networks were developed. Streams in a river converge to generate larger streams. However, smaller streams can merge to form bigger streams of any size. The so-called Horton-Strahler order can be used to investigate the networks of rivers with a topological structure. Every branch of the network is given an integer number under this system. Larger numbers correspond to the network's larger stream segments, and they reflect various levels of the branch hierarchy. The statistical characteristics of river networks, particularly the discovery that river networks are fractal, are described in terms of the Horton-Strahler ordering. Furthermore, Tokunaga's original side-branching statistics can be utilized to describe both the general characteristics of river networks and their deviations.

The literature contains a variety of grouping methods for the classification of lung vasculature. Examples of widely used metrics to categorize human airway and pulmonary artery branching include generations, orders, Strahler order, and the aforementioned fractal branching as a technique targeted specifically at the categorization of monopodial lungs. These methods are typically proven by demonstrating a link (often logarithmic) between a group designation and the mean dimension of one or more morphological features (for example, diameter or length). Other research used one technique (for instance, orders) and used the findings to describe branching variations between species. When a method's suitability for a given task is regarded to be inappropriate because a type of separate vessel is classified into a broad range of generations, comparisons between other ways are uncommon and only made in debate form. Because of the various geometric presumptions used to create the classifications, the resulting groups will exhibit varying degrees of internal morphometric similarity and will vary in size and number. This begs the question of whether the classification systems would work best for the monopodial lung and whether there are any other systems for categorizing the pulmonary artery branches that would be better than the ones that are now used.

The Strahler method has gained wide acceptance, especially in lung morphometric analysis [153,185,188]. A useful tool for identifying and comparing morphologically and functionally similar structures, such as between healthy and sick tissue, is the classification of the segments of the vascular tree into homogenous groups. Learning site-specific information regarding the preferential localization of ongoing processes may provide a thorough characterization of developmental or pathological processes. This could aid in extending current techniques for studying the pulmonary vasculature in the lung to more thoroughly examine the consequences and progression of other conditions like cystic fibrosis, bronchopulmonary dysplasia, or chronic obstructive pulmonary disease. Since there are abdominal organs on one side of the thorax, pooling of the data would eventually result in bias and confounding, therefore, both lungs were analyzed separately. Concerning the parameter selection, the number of branches and generations, vessel diameters, and lengths were included. So, the selection bias, as mentioned above, was prevented. Four levels of branching were demonstrated in each lung in both groups similar to the other studies in the literature. Both lungs in CDH were found to be affected historically

regardless of the hernia side [202]. The comparison of both sides of the lung in healthy and CDH fetuses also correlates with this information. While one can speculate that, it is not new information, it is definitely a novel finding that a non-invasive tool could demonstrate it and have that tool the potential to be translated into human counterparts.

In the most distal segments and elements of the vessels, there was a statistically significant difference. The 2nd and 3rd segments of the right lung were likewise discovered to be significantly different, but no such change was found in the left lung, where the herniation occurred. In addition, the lengths of segments and elements were found to be comparable among groups. The disturbed fractal structure in CDH fetuses was convincingly proven in terms of the element number when the tree structure of the lungs was studied according to Horton's law. However, the length of the elements could not indicate this, which could be the reason for the fetal vascular tree's immaturity. The distal vasculature had a statistically significant difference when the ramification of the vascular tree was examined, which was consistent with the typical findings of CDH. The connectivity matrix depicts the average branching numbers between vessels of all orders in an arterial tree and is a useful tool for calculating estimated blood pressure and vascular volume in the coronary arteries [156]. When the connection matrix was viewed as a whole, no statistical significance could be found between groups, although there were fewer elements of order 1 in the CDH group that sprang from elements of order 1 on the left and fewer components of order 1 that sprang from elements of order 3 on the right.

Micro-CT has unfortunate constraints that go beyond the fact that it is an ex-vivo technology, especially in the equipment and experiment setup and design [203]. To reduce radiation exposure, conversion of these investigations into in-vivo MRI images has been attempted. The image quality, just like with conventional imaging modalities, depends on minimizing artifacts from improper positioning or interference. For accurate 3-dimensional reconstruction, precise geometric proportions must be followed [203]. This might be accomplished by using pins to secure the specimens to the scanner. Both PFA 4% and Lugol-induced tissue shrinking are limiting factors that may change the tissue's architecture. According to Vickerton et al., the shrinking effect of the Lugol is primarily concentration-dependent. To avoid this, we took advantage of the earlier-adjusted concentration [204]. Comparing specific branching patterns between fetal samples and recognizing them, on the other hand, requires the use of micro-CT, which is the greatest imaging technology available. Identification of illness influence on embryological and developmental state requires determination of organ-specific vascularization patterns and modeling of these vascular trees. The commercial software used in the field has also limitations since most of them are operator dependent.

8. Conclusions

1. Our research demonstrates a marked decrease in arterial branching in the lungs of fetuses diagnosed with CDH, indicating a direct correlation between the extent of vascular development and the severity of pulmonary hypoplasia.
2. The use of advanced radiological imaging techniques has been validated as an effective method for identifying the fetal lung vascular tree, offering a promising approach to estimate the potential degree of pulmonary hypertension.
3. This study supports the feasibility of assessing the severity of CDH prenatally through radiological evaluation, providing critical information for parental counseling and the development of prenatal therapeutic strategies aimed at mitigating postnatal complications associated with the disease.

9. Future lines

The upcoming studies that we are working on are to translate this knowledge into humans. Utilizing similar techniques to prenatal MRI and correlating it with postnatal CT, echocardiography and the outcome of the patient will potentially result in creating an artificial intelligence-based prenatal parameter to predict the survival of the fetuses.

10. Bibliography

[1] Bhutta Z, Das J, Bahl R. Erratum: The Lancet every Newborn study group. Can available interventions end preventable deaths in mothers, newborn babies, and stillbirths, and at what cost? (The Lancet (2014) 384 (347-370)). Lancet 2014. https://doi.org/10.1016/S0140-6736(14)61241-1.

[2] WHO. Children: improving survival and well-being. Fact Sheets 2019.

[3] Institute of Health Metrics and Evaluation. GBD Results Tool. Institue Heal Metrics Eval 2019.

[4] The Institute for Health Metrics and Evaluation. The Institute for Health Metrics and Evaluation (IHME). Inst Heal Metrics Eval 2018.

[5] Wright NJ, Anderson JE, Ozgediz D, Farmer DL, Banu T. Addressing paediatric surgical care on World Birth Defects Day. Lancet 2018. https://doi.org/10.1016/s0140-6736(18)30501-4.

[6] Wang H, Bhutta ZA, Coates MM, Coggeshall M, Dandona L, Diallo K, et al. Erratum: Global, regional, national, and selected subnational levels of stillbirths, neonatal, infant, and under-5 mortality, 1980–2015: a systematic analysis for the Global Burden of Disease Study 2015 (The Lancet (2016) 388(10053) (1725–1774)(S014067361. Lancet 2017. https://doi.org/10.1016/S0140-6736(16)32608-3.

[7] Erratum: First reported cases of anti-NMDA receptor encephalitis in Vietnamese adolescents and adults: Global, regional, and national incidence, prevalence, and years lived with disability for 310 diseases and injuries, 1990–2015: a systematic analysis fo. Lancet 2017. https://doi.org/10.1016/S0140-6736(16)32606-X.

[8] Sitkin NA, Ozgediz D, Donkor P, Farmer DL. Congenital anomalies in low- and middle-income countries:The unborn child of global surgery. World J Surg 2015. https://doi.org/10.1007/s00268-014-2714-9.

[9] Watanabe ME. The United Nations Sustainable Development Goals. Bioscience 2020. https://doi.org/10.1093/biosci/biz155.

[10] Ettorre E. Reproductive genetics, gender and the body: “Please doctor, may I have a normal baby?” Sociology 2000. https://doi.org/10.1177/s0038038500000262.

[11] Allyse M, Minear MA, Berson E, Sridhar S, Rote M, Hung A, et al. Non-invasive prenatal testing: A review of international implementation and challenges. Int J Womens Health 2015. https://doi.org/10.2147/IJWH.S67124.

[12] Galeva S, Gil MM, Konstantinidou L, Akolekar R, Nicolaides KH. First-trimester screening for trisomies by cfDNA testing of maternal blood in singleton and twin pregnancies: factors affecting test failure. Ultrasound Obstet Gynecol 2019. https://doi.org/10.1002/uog.20290.

[13] Gregg AR, Gross SJ, Best RG, Monaghan KG, Bajaj K, Skotko BG, et al. ACMG statement on noninvasive prenatal screening for fetal aneuploidy. Genet Med 2013. https://doi.org/10.1038/gim.2013.29.

[14] Graves CE, Harrison MR, Padilla BE. Minimally Invasive Fetal Surgery. Clin Perinatol 2017. https://doi.org/10.1016/j.clp.2017.08.001.

[15] Neher G. LEONARDO LEONARDO DA VINCI. THE FLIGHTS OF THE MIND. Art B 2005;12:59–59. https://doi.org/10.1111/j.1467-8357.2005.555_4.x.

[16] Vesalius A, Calcar JS van, Holbein H, Oporinus J. De humani corporis fabrica libri septem.

Basileae Bruxelles 1543.

[17] Jancelewicz T, Harrison MR. A History of Fetal Surgery. Clin Perinatol 2009. https://doi.org/10.1016/j.clp.2009.03.007.

[18] Rosenkrantz JG, Simon RC, Carlisle JH. Fetal surgery in the pig with a review of other mammalian fetal technics. J Pediatr Surg 1968. https://doi.org/10.1016/0022-3468(68)90345-X.

[19] Louw JH, Barnard CN. CONGENITAL INTESTINAL ATRESIA OBSERVATIONS ON ITS ORIGIN. Lancet 1955. https://doi.org/10.1016/S0140-6736(55)92852-X.

[20] Ohi R, Suzuki H, Kato T, Kasai M. Development of the lung in fetal rabbits with experimental diaphragmatic hernia. J Pediatr Surg 1976. https://doi.org/10.1016/S0022-3468(76)80073-5.

[21] Thomasson BH, Esterly JR, Ravitch MM. Morphologic changes in the fetal rabbit kidney after intrauterine ureteral ligation. Invest Urol 1970.

[22] Beck AD. The effect of intra-uterine urinary obstruction upon the development of the fetal kidney. J Urol 1971. https://doi.org/10.1016/S0022-5347(17)61629-X.

[23] Suzuki K, Plentl AA. Chronic implantation of instruments in the neck of the primate fetus for physiologic studies and production of hydramnios. Am J Obstet Gynecol 1969. https://doi.org/10.1016/S0002-9378(16)34401-5.

[24] Adzick NS, Outwater KM, Harrison MR, Davies P, Glick PL, deLorimier AA, et al. Correction of congenital diaphragmatic hernia in utero IV. An early gestational fetal lamb model for pulmonary vascular morphometric analysis. J Pediatr Surg 1985;20:673–80. https://doi.org/10.1016/S0022-3468(85)80022-1.

[25] Harrison MR, Keller RL, Hawgood SB, Kitterman JA, Sandberg PL, Farmer DL, et al. A Randomized Trial of Fetal Endoscopic Tracheal Occlusion for Severe Fetal Congenital Diaphragmatic Hernia. N Engl J Med 2003. https://doi.org/10.1056/NEJMoa035005.

[26] Sherer DM. Is fetal hydronephrosis overdiagnosed? Ultrasound Obstet Gynecol 2000. https://doi.org/10.1046/j.1469-0705.2000.00339.x.

[27] Adzick NS. Prospects for fetal surgery. Early Hum Dev 2013. https://doi.org/10.1016/j.earlhumdev.2013.09.010.

[28] AYDIN E. Current Approach for Prenatally Diagnosed Congenital Anomalies That Requires Surgery. Turkiye Klin J Gynecol Obstet 2016. https://doi.org/10.5336/gynobstet.2016-53316.

[29] Caraiani C, Dong Y, Rudd AG, Dietrich CF. Reasons for inadequate or incomplete imaging techniques. Med Ultrason 2018. https://doi.org/10.11152/mu-1736.

[30] Helmy S, Bader Y, Koch M, Tiringer D, Kollmann C. Measurement of thermal effects of doppler ultrasound: An in vitro study. PLoS One 2015. https://doi.org/10.1371/journal.pone.0135717.

[31] Schittny JC. Development of the lung. Cell Tissue Res 2017. https://doi.org/10.1007/s00441-016-2545-0.

[32] Harding R, Hooper SB. Regulation of lung expansion and lung growth before birth. J Appl Physiol 1996. https://doi.org/10.1152/jappl.1996.81.1.209.

[33] Rubaltelli FF, Bonafè L, Tangucci M, Spagnolo A, Dani C. Epidemiology of neonatal acute respiratory disorders. A multicenter study on incidence and fatality rates of neonatal acute respiratory disorders according to gestational age, maternal age, pregnancy complications and

type of delivery. Biol Neonate 1998;74:7–15. https://doi.org/10.1159/000014005.

[34] Knox WF, Barson AJ. Pulmonary hypoplasia in a regional perinatal unit. Early Hum Dev 1986;14:33–42. https://doi.org/10.1016/0378-3782(86)90167-2.

[35] Moessinger AC, Santiago A, Paneth NS, Rey HR, Blanc WA, Jr JMD. Time-trends in necropsy prevalence and birth prevalence of lung hypoplasia. Paediatr Perinat Epidemiol 1989;3:421–31. https://doi.org/10.1111/j.1365-3016.1989.tb00529.x.

[36] Laudy JAM, Wladimiroff JW. The fetal lung 2: Pulmonary hypoplasia. Ultrasound Obstet Gynecol 2000;16:482–94. https://doi.org/10.1046/j.1469-0705.2000.00252.x.

[37] Husain AN, Hessel RG. Neonatal pulmonary hypoplasia: An autopsy study of 25 cases. Fetal Pediatr Pathol 1993;13:475–84. https://doi.org/10.3109/15513819309048237.

[38] Page D V., Stocker JT. Anomalies associated with pulmonary hypoplasia. Am Rev Respir Dis 1982;125:216–21. https://doi.org/10.1164/arrd.1982.125.2.216.

[39] Wigglesworth JS. J. of Hospital, 1980:264–7.

[40] Bridges JP, Lin S, Ikegami M, Shannon JM. Conditional hypoxia inducible factor-1α induction in embryonic pulmonary epithelium impairs maturation and augments lymphangiogenesis. Dev Biol 2012;362:24–41. https://doi.org/10.1016/j.ydbio.2011.10.033.

[41] Tuder RM, Cool CD, Yeager M, Taraseviciene-Stewart L, Bull TM, Voelkel NF. The pathobiology of pulmonary hypertension: Endothelium. Clin Chest Med 2001;22:405–18. https://doi.org/10.1016/S0272-5231(05)70280-X.

[42] Ameis D, Khoshgoo N, Keijzer R. Abnormal lung development in congenital diaphragmatic hernia. Semin Pediatr Surg 2017. https://doi.org/10.1053/j.sempedsurg.2017.04.011.

[43] Areechon W, Reid L. Hypoplasia of lung with congenital diaphragmatic hernia. Br Med J 1963. https://doi.org/10.1136/bmj.1.5325.230.

[44] McCabe AJ, Carlino U, Holm BA, Glick PL. Upregulation of keratinocyte growth factor in the tracheal ligation lamb model of congenital diaphragmatic hernia. J. Pediatr. Surg., 2001. https://doi.org/10.1053/jpsu.2001.20029.

[45] Aydin E, Lim F-Y, Kingma P, Haberman B, Rymeski B, Burns P, et al. Congenital diaphragmatic hernia: the good, the bad, and the tough. Pediatr Surg Int 2019. https://doi.org/10.1007/s00383-019-04442-z.

[46] Colvin J, Bower C, Dickinson JE, Sokol J. Outcomes of congenital diaphragmatic hernia: a population-based study in Western Australia. Pediatrics 2005;116:e356-63. https://doi.org/10.1542/peds.2004-2845.

[47] McGivern MR, Best KE, Rankin J, Wellesley D, Greenlees R, Addor M-C, et al. Epidemiology of congenital diaphragmatic hernia in Europe: a register-based study. Arch Dis Child Fetal Neonatal Ed 2015;100:F137-44. https://doi.org/10.1136/archdischild-2014-306174.

[48] Gallot D, Boda C, Ughetto S, Perthus I, Robert-Gnansia E, Francannet C, et al. Prenatal detection and outcome of congenital diaphragmatic hernia: A French registry-based study. Ultrasound Obstet Gynecol 2007;29:276–83. https://doi.org/10.1002/uog.3863.

[49] Yang W, Carmichael SL, Harris JA, Shaw GM. Epidemiologic characteristics of congenital diaphragmatic hernia among 2.5 million California births, 1989-1997. Birth Defects Res Part A - Clin Mol Teratol 2006;76:170–4. https://doi.org/10.1002/bdra.20230.

[50] Tennant PWG, Samarasekera SD, Pless-Mulloli T, Rankin J. Sex differences in the prevalence of congenital anomalies: A population-based study. Birth Defects Res Part A - Clin Mol Teratol 2011;91:894–901. https://doi.org/10.1002/bdra.22846.

[51] Zani A, Zani-Ruttenstock E, Pierro A. Advances in the surgical approach to congenital diaphragmatic hernia. Semin Fetal Neonatal Med 2014;19:364–9. https://doi.org/10.1016/j.siny.2014.09.002.

[52] Tovar JA, Irish M, Holm B, Glick P, Golombek S, McNamara J, et al. Congenital Diaphragmatic Hernia. Orphanet J Rare Dis 2012;7:1. https://doi.org/10.1186/1750-1172-7-1.

[53] Wright NJ, Wright N, Ade-Ajayi N, Ademuyiwa A, Ameh E, Davies J, et al. Management and outcomes of gastrointestinal congenital anomalies in low, middle and high income countries: Protocol for a multicentre, international, prospective cohort study. BMJ Open 2019;9. https://doi.org/10.1136/bmjopen-2019-030452.

[54] Nolan H, Aydin E, Frischer JS, Peiro JL, Rymeski B, Lim F-Y. Hemorrhage after on-ECMO repair of CDH is equivalent for muscle flap and prosthetic patch. J Pediatr Surg 2019;54. https://doi.org/10.1016/j.jpedsurg.2019.04.025.

[55] Aydın E, Özler O, Burns P, Lim F-Y, Peiró JL. Left congenital diaphragmatic hernia-associated musculoskeletal deformities. Pediatr Surg Int 2019;35. https://doi.org/10.1007/s00383-019-04548-4.

[56] Aydın E, Nolan H, Peiró JL, Burns P, Rymeski B, Lim FY. When primary repair is not enough: a comparison of synthetic patch and muscle flap closure in congenital diaphragmatic hernia? Pediatr Surg Int 2020. https://doi.org/10.1007/s00383-020-04634-y.

[57] Logan J, Rice H, Goldberg R, Cotten C. Congenital diaphragmatic hernia: a systematic review and summary of best-evidence practice strategies. J Perinatol 2007;27:535–49.

[58] Brownlee EM, Howatson AG, Davis CF, Sabharwal AJ. The hidden mortality of congenital diaphragmatic hernia: a 20-year review. J Pediatr Surg 2009;44:317–20. https://doi.org/10.1016/j.jpedsurg.2008.10.076.

[59] Keijzer R, Liu J, Deimling J, Tibboel D, Post M. Dual-hit hypothesis explains pulmonary hypoplasia in the nitrofen model of congenital diaphragmatic hernia. Am J Pathol 2000;156:1299–306. https://doi.org/10.1016/S0002-9440(10)65000-6.

[60] Metkus AP, Filly RA, Stringer MD, Harrison MR, Adzick NS. Sonographic predictors of survival in fetal diaphragmatic hernia. J. Pediatr. Surg., vol. 31, 1996, p. 148–52. https://doi.org/10.1016/S0022-3468(96)90338-3.

[61] Harrison MR, Mychaliska GB, Albanese CT, Jennings RW, Farrell JA, Hawgood S, et al. Correction of congenital diaphragmatic hernia in utero IX: Fetuses with poor prognosis (liver herniation and low lung-to-head ratio) can be saved fetoscopic temporary tracheal occlusion. J. Pediatr. Surg., vol. 33, 1998, p. 1017–23. https://doi.org/10.1016/S0022-3468(98)90524-3.

[62] Harrison MR, Sydorak RM, Farrell JA, Kitterman JA, Filly RA, Albanese CT. Fetoscopic temporary tracheal occlusion for congenital diaphragmatic hernia: Prelude to a randomized, controlled trial. J Pediatr Surg 2003;38:1012–20. https://doi.org/10.1016/S0022-3468(03)00182-9.

[63] Deprest J, Gratacos E, Nicolaides KH. Fetoscopic tracheal occlusion (FETO) for severe congenital diaphragmatic hernia: Evolution of a technique and preliminary results. Ultrasound Obstet Gynecol 2004;24:121–6. https://doi.org/10.1002/uog.1711.

[64] Harrison MR, Adzick NS, Flake AW, VanderWall KJ, Bealer JF, Howell LJ, et al. Correction of congenital diaphragmatic hernia in utero VIII: Response of the hypoplastic lung to tracheal occlusion. J Pediatr Surg 1996;31:1339–48. https://doi.org/10.1016/S0022-3468(96)90824-6.

[65] Flake AW, Crombleholme TM, Johnson MP, Howell LJ, Adzick NS. Treatment of severe congenital diaphragmatic hernia by fetal tracheal occlusion: Clinical experience with fifteen cases. Am. J. Obstet. Gynecol., 2000. https://doi.org/10.1067/mob.2000.108871.

[66] Laudy JAM, Van Gucht M, Van Dooren MF, Wladimiroff JW, Tibboel D. Congenital diaphragmatic hernia: An evaluation of the prognostic value of the lung-to-head ratio and other prenatal parameters. Prenat Diagn 2003;23:634–9. https://doi.org/10.1002/pd.654.

[67] Heling KS, Wauer RR, Hammer H, Bollmann R, Chaoui R. Reliability of the lung-to-head ratio in predicting outcome and neonatal ventilation parameters in fetuses with congenital diaphragmatic hernia. Ultrasound Obstet Gynecol 2005;25:112–8. https://doi.org/10.1002/uog.1837.

[68] Quintero RA, Quintero LF, Chmait R, Gómez Castro L, Korst LM, Fridman M, et al. The quantitative lung index (QLI): A gestational ageindependent sonographic predictor of fetal lung growth. Am J Obstet Gynecol 2011;205:544.e1-544.e8. https://doi.org/10.1016/j.ajog.2011.07.031.

[69] Jani J, Cannie M, Sonigo P, Robert Y, Moreno O, Benachi A, et al. Value of prenatal magnetic resonance imaging in the prediction of postnatal outcome in fetuses with diaphragmatic hernia. Ultrasound Obstet Gynecol 2008;32:793–9. https://doi.org/10.1002/uog.6234.

[70] Büsing KA, Kilian AK, Schaible T, Debus A, Weiss C, Neff KW. Reliability and validity of MR image lung volume measurement in fetuses with congenital diaphragmatic hernia and in vitro lung models. Radiology 2008;246:553–61. https://doi.org/10.1148/radiol.2462062166.

[71] Kastenholz KE, Weis M, Hagelstein C, Weiss C, Kehl S, Schaible T, et al. Correlation of observed-to-expected MRI fetal lung volume and ultrasound lung-to-head ratio at different gestational times in fetuses with congenital diaphragmatic hernia. Am J Roentgenol 2016;206:856–66. https://doi.org/10.2214/AJR.15.15018.

[72] Rypens F, Metens T, Rocourt N, Sonigo P, Brunelle F, Quere MP, et al. Fetal lung volume: Estimation at MR imaging - Initial results. Radiology 2001;219:236–41. https://doi.org/10.1148/radiology.219.1.r01ap18236.

[73] Jani JC, Cannie M, Peralta CFA, Deprest JA, Nicolaides KH, Dymarkowski S. Lung volumes in fetuses with congenital diaphragmatic hernia: Comparison of 3D US and MR imaging assessments. Radiology 2007;244:575–82. https://doi.org/10.1148/radiol.2442061158.

[74] Jani J, Cannie M, Done E, Van Mieghem T, Van Schoubroeck D, Gucciardo L, et al. Relationship between lung area at ultrasound examination and lung volume assessment with magnetic resonance imaging in isolated congenital diaphragmatic hernia. Ultrasound Obstet Gynecol 2007;30:855–60. https://doi.org/10.1002/uog.5168.

[75] Strizek B, Cos Sanchez T, Khalifé J, Jani J, Cannie M. Impact of operator experience on the variability of fetal lung volume estimation by 3D-ultrasound (VOCAL) and magnetic resonance imaging in fetuses with congenital diaphragmatic hernia. J Matern Neonatal Med 2015;28:858–64. https://doi.org/10.3109/14767058.2014.935760.

[76] Barnewolt CE, Kunisaki SM, Fauza DO, Nemes LP, Estroff JA, Jennings RW. Percent predicted lung volumes as measured on fetal magnetic resonance imaging: a useful biometric parameter for risk stratification in congenital diaphragmatic hernia. J Pediatr Surg 2007;42:193–7. https://doi.org/10.1016/j.jpedsurg.2006.09.018.

[77] Meyers ML, Garcia JR, Blough KL, Zhang W, Cassady CI, Mehollin-Ray AR. Fetal lung volumes by MRI: Normal weekly values from 18 through 38 weeks' gestation. Am J Roentgenol 2018;211:432–8. https://doi.org/10.2214/AJR.17.19469.

[78] Piehler JM, Danielson GK, McGoon DC, Wallace RB, Fulton RE, Mair DD. Management of pulmonary atresia with ventricular septal defect and hypoplastic pulmonary arteries by right ventricular outflow construction. J Thorac Cardiovasc Surg 1980;80:552–67. https://doi.org/10.1016/s0022-5223(19)37742-6.

[79] Nakata S, Imai Y, Takanashi Y, Kurosawa H, Tezuka K, Nakazawa M, et al. A new method for the quantitative standardization of cross-sectional areas of the pulmonary arteries in congenital heart diseases with decreased pulmonary blood flow. J Thorac Cardiovasc Surg 1984;88:610–9. https://doi.org/10.1016/s0022-5223(19)38300-x.

[80] Luo Q, He X, Song Z, Zhang X, Tong Z, Shen J, et al. Preoperative Morphological Prediction of Early Reoperation Risk After Primary Repair in Tetralogy of Fallot: A Contemporary Analysis of 83 Cases. Pediatr Cardiol 2021;42:1512–25. https://doi.org/10.1007/s00246-021-02635-9.

[81] Yang XY, Jing XY, Chen Z, Li L, Fan XM, Su JW. A summary of second systemic pulmonary shunt for congenital heart disease with pulmonary hypoxemia. J Cardiothorac Surg 2020;15. https://doi.org/10.1186/s13019-020-01132-z.

[82] Xiang Y, Cheng G, Jin K, Zhang X, Yang Y. Computed tomography findings and preoperative risk factors for mortality of total anomalous pulmonary venous connection. Int J Cardiovasc Imaging 2018;34:1969–75. https://doi.org/10.1007/s10554-018-1405-2.

[83] Takahashi S, Oishi Y, Ito N, Nanba Y, Tsukamoto K, Nakamura T, et al. Evaluating mortality and disease severity in congenital diaphragmatic hernia using the McGoon and pulmonary artery indices. J Pediatr Surg 2009;44:2101–6. https://doi.org/10.1016/j.jpedsurg.2009.05.012.

[84] Suda K, Bigras JL, Bohn D, Hornberger LK, McCrindle BW. Echocardiographic predictors of outcome in newborns with congenital diaphragmatic hernia. Pediatrics 2000;105:1106–9. https://doi.org/10.1542/peds.105.5.1106.

[85] Casaccia G, Crescenzi F, Dotta A, Capolupo I, Braguglia A, Danhaive O, et al. Birth weight and McGoon Index predict mortality in newborn infants with congenital diaphragmatic hernia. J Pediatr Surg 2006;41:25–8. https://doi.org/10.1016/j.jpedsurg.2005.10.002.

[86] Vuletin JF, Lim FY, Cnota J, Kline-Fath B, Salisbury S, Haberman B, et al. Prenatal pulmonary hypertension index: novel prenatal predictor of severe postnatal pulmonary artery hypertension in antenatally diagnosed congenital diaphragmatic hernia. J Pediatr Surg 2010;45:703–8. https://doi.org/10.1016/j.jpedsurg.2009.11.013.

[87] Zerhouni S, Mayer C, Skarsgard ED. Can we select fetuses with intra-abdominal calcification for delivery in neonatal surgical centres? J Pediatr Surg 2013;48:946–50. https://doi.org/10.1016/j.jpedsurg.2013.02.006.

[88] Albanese CT, Lopoo J, Goldstein RB, Filly RA, Feldstein VA, Calen PW, et al. Fetal liver position and perinatal outcome for congenital diaphragmatic hernia. Prenat Diagn 1998;18:1138–42.

[89] Fumino S, Shimotake T, Kume Y, Tsuda T, Aoi S, Kimura O, et al. A clinical analysis of prognostic parameters of survival in children with congenital diaphragmatic hernia. Eur J Pediatr Surg 2005;15:399–403. https://doi.org/10.1055/s-2005-872925.

[90] Jani J, Keller RL, Benachi A, Nicolaides KH, Favre R, Gratacos E, et al. Prenatal prediction of survival in isolated left-sided diaphragmatic hernia. Ultrasound Obstet Gynecol 2006;27:18–22.

https://doi.org/10.1002/uog.2688.

[91] Kitano Y, Nakagawa S, Kuroda T, Honna T, Itoh Y, Nakamura T, et al. Liver position in fetal congenital diaphragmatic hernia retains a prognostic value in the era of lung-protective strategy. J Pediatr Surg 2005;40:1827–32. https://doi.org/10.1016/j.jpedsurg.2005.08.020.

[92] Hedrick HL, Danzer E, Merchant A, Bebbington MW, Zhao H, Flake AW, et al. Liver position and lung-to-head ratio for prediction of extracorporeal membrane oxygenation and survival in isolated left congenital diaphragmatic hernia. Am J Obstet Gynecol 2007;197. https://doi.org/10.1016/j.ajog.2007.07.001.

[93] Cannie M, Jani J, Chaffiotte C, Vaast P, Deruelle P, Houfflin-Debarge V, et al. Quantification of intrathoracic liver herniation by magnetic resonance imaging and prediction of postnatal survival in fetuses with congenital diaphragmatic hernia. Ultrasound Obstet Gynecol 2008;32:627–32. https://doi.org/10.1002/uog.6146.

[94] Ruano R, Lazar DA, Cass DL, Zamora IJ, Lee TC, Cassady CI, et al. Fetal lung volume and quantification of liver herniation by magnetic resonance imaging in isolated congenital diaphragmatic hernia. Ultrasound Obstet Gynecol 2014;43. https://doi.org/10.1002/uog.13223.

[95] Jani JC, Benachi A, Nicolaides KH, Allegaert K, Gratacó E, Mazkereth R, et al. Prenatal prediction of neonatal morbidity in survivors with congenital diaphragmatic hernia: A multicenter study. Ultrasound Obstet Gynecol 2009;33:64–9. https://doi.org/10.1002/uog.6141.

[96] Keijzer R, Puri P. Congenital diaphragmatic hernia. Semin Pediatr Surg 2010;19:180–5. https://doi.org/S1055-8586(10)00014-4 [pii]\r10.1053/j.sempedsurg.2010.03.001.

[97] Grizelj R, Bojanić K, Vuković J, Novak M, Weingarten TN, Schroeder DR, et al. Hernia Sac Presence Portends Better Survivability of Isolated Congenital Diaphragmatic Hernia with "Liver-Up." Am J Perinatol 2017;34:515–9. https://doi.org/10.1055/s-0036-1593765.

[98] Zamora IJ, Cass DL, Lee TC, Welty S, Cassady CI, Mehollin-Ray AR, et al. The presence of a hernia sac in congenital diaphragmatic hernia is associated with better fetal lung growth and outcomes. J Pediatr Surg 2013;48:1165–71. https://doi.org/10.1016/j.jpedsurg.2013.03.010.

[99] Spaggiari E, Stirnemann J, Bernard JP, De Saint Blanquat L, Beaudoin S, Ville Y. Prognostic value of a hernia sac in congenital diaphragmatic hernia. Ultrasound Obstet Gynecol 2013;41:286–90. https://doi.org/10.1002/uog.11189.

[100] Papadakis K, De Paepe ME, Tackett LD, Piasecki GJ, Luks FI. Temporary tracheal occlusion causes catch-up lung maturation in a fetal model of diaphragmatic hernia. J. Pediatr. Surg., vol. 33, 1998, p. 1030–7. https://doi.org/10.1016/S0022-3468(98)90526-7.

[101] Kitano Y, Kanai M, Davies P, Von Allmen D, Yang EY, Radu A, et al. Lung growth induced by prenatal tracheal occlusion and its modifying factors: A study in the rat model of congenital diaphragmatic hernia. J. Pediatr. Surg., vol. 36, 2001, p. 251–9. https://doi.org/10.1053/jpsu.2001.20683.

[102] Mychaliska GB, Bealer JF, Graf JL, Rosen MA, Adzick NS, Harrison MR. Operating on placental support: The ex utero intrapartum treatment procedure. J. Pediatr. Surg., vol. 32, 1997, p. 227–31. https://doi.org/10.1016/S0022-3468(97)90184-6.

[103] Bouchard S, Johnson MP, Flake AW, Howell LJ, Myers LB, Adzick NS, et al. The EXIT procedure: Experience and outcome in 31 cases. J Pediatr Surg 2002. https://doi.org/10.1053/jpsu.2002.30839.

[104] Bettman RB, Hess JH. Incarcerated diaphragmatic hernia in an infant, with operation and recovery. J Am Med Assoc 1929;92:2014–6. https://doi.org/10.1001/jama.1929.92700500001009.

[105] Snoek KG, Reiss IKM, Greenough A, Capolupo I, Urlesberger B, Wessel L, et al. Standardized postnatal management of infants with congenital diaphragmatic hernia in Europe: The CDH EURO Consortium Consensus - 2015 Update. Neonatology 2016;110:66–74. https://doi.org/10.1159/000444210.

[106] Hutcheon JA, Butler B, Lisonkova S, Marquette GP, Mayer C, Skoll A, et al. Timing of delivery for pregnancies with congenital diaphragmatic hernia. BJOG An Int J Obstet Gynaecol 2010;117:1658–62. https://doi.org/10.1111/j.1471-0528.2010.02738.x.

[107] Odibo AO, Najaf T, Vachharajani A, Warner B, Mathur A, Warner BW. Predictors of the need for extracorporeal membrane oxygenation and survival in congenital diaphragmatic hernia: A center's 10-year experience. Prenat Diagn 2010;30:518–21. https://doi.org/10.1002/pd.2508.

[108] Safavi A, Lin Y, Skarsgard ED. Perinatal management of congenital diaphragmatic hernia: When and how should babies be delivered? Results from the Canadian Pediatric Surgery Network. J Pediatr Surg 2010;45:2334–9. https://doi.org/10.1016/j.jpedsurg.2010.08.026.

[109] Boucherat O, Benachi A, Chailley-Heu B, Franco-Montoya ML, Elie C, Martinovic J, et al. Surfactant maturation is not delayed in human fetuses with diaphragmatic hernia. PLoS Med 2007;4:1205–15. https://doi.org/10.1371/journal.pmed.0040237.

[110] Partridge EA, Peranteau WH, Rintoul NE, Herkert LM, Flake AW, Adzick NS, et al. Timing of repair of congenital diaphragmatic hernia in patients supported by extracorporeal membrane oxygenation (ECMO). J Pediatr Surg 2015;50:260–2. https://doi.org/10.1016/j.jpedsurg.2014.11.013.

[111] Ye LF, Fan Y, Shu Q, Lin R. Management of persistent pulmonary hypertension in newborns with ECMO support: a single center's experience. World J Pediatr 2019;15:100–3. https://doi.org/10.1007/s12519-018-0215-x.

[112] Harrington KP, Goldman AP. The role of extracorporeal membrane oxygenation in congenital diaphragmatic hernia. Semin Pediatr Surg 2005;14:72–6. https://doi.org/10.1053/j.sempedsurg.2004.10.028.

[113] Longer JC, Harrison MR, Adzick NS. Congenital diaphragmatic hernia: Current controversies in prenatal and postnatal management. Fetal Diagn Ther 1987;2:209–15. https://doi.org/10.1159/000263319.

[114] Puligandla PS, Grabowski J, Austin M, Hedrick H, Renaud E, Arnold M, et al. Management of congenital diaphragmatic hernia: A systematic review from the APSA outcomes and evidence based practice committee. J Pediatr Surg 2015;50:1958–70. https://doi.org/10.1016/j.jpedsurg.2015.09.010.

[115] Kane JM, Harbert J, Hohmann S, Pillai S, Behal R, Selip D, et al. Case Volume and Outcomes of Congenital Diaphragmatic Hernia Surgery in Academic Medical Centers. Am J Perinatol 2015;32:845–52. https://doi.org/10.1055/s-0034-1543980.

[116] Fallon SC, Cass DL, Olutoye OO, Zamora IJ, Lazar DA, Larimer EL, et al. Repair of congenital diaphragmatic hernias on Extracorporeal Membrane Oxygenation (ECMO): Does early repair improve patient survival? J. Pediatr. Surg., vol. 48, 2013, p. 1172–6. https://doi.org/10.1016/j.jpedsurg.2013.03.008.

[117] Aydin E, Torlak N, Haberman B, Lim FY, Peiro JL. The Survivorship Bias in Congenital

Diaphragmatic Hernia. Children 2022;9. https://doi.org/10.3390/children9020218.

[118] Chandrasekharan PK, Rawat M, Madappa R, Rothstein DH, Lakshminrusimha S. Congenital diaphragmatic hernia - a review. Matern Heal Neonatol Perinatol 2017;3. https://doi.org/10.1186/s40748-017-0045-1.

[119] Quinney M, Wellesley H. Anaesthetic management of patients with a congenital diaphragmatic hernia. BJA Educ 2018;18:95–101. https://doi.org/10.1016/j.bjae.2018.01.001.

[120] Koziarkiewicz M, Taczalska A, Piaseczna-Piotrowska A. Long-term follow-up of children with congenital diaphragmatic hernia-observations from a single institution. Eur J Pediatr Surg 2014;24:500–7. https://doi.org/10.1055/s-0033-1357751.

[121] Chen C, Friedman S, Butler S, Jeruss S, Terrin N, Tighiouart H, et al. Approaches to neurodevelopmental assessment in congenital diaphragmatic hernia survivors. J Pediatr Surg 2007;42:1052–6. https://doi.org/10.1016/j.jpedsurg.2007.01.042.

[122] Postdischarge Follow-Up of Infants With Congenital Diaphragmatic Hernia. Pediatr. Clin. Pract. Guidel. Policies, 2021, p. 1469–1469. https://doi.org/10.1542/9781610020862-part05-postdischarge.

[123] Trachsel D, Selvadurai H, Bohn D, Langer JC, Coates AL. Long-term pulmonary morbidity in survivors of congenital diaphragmatic hernia. Pediatr Pulmonol 2005;39:433–9. https://doi.org/10.1002/ppul.20193.

[124] Muratore CS, Kharasch V, Lund DP, Sheils C, Friedman S, Brown C, et al. Pulmonary morbidity in 100 survivors of congenital diaphragmatic hernia monitored in a multidisciplinary clinic. J Pediatr Surg 2001;36:133–40. https://doi.org/10.1053/jpsu.2001.20031.

[125] Tan JK, Banton G, Minutillo C, Hall GL, Wilson A, Murray C, et al. Long-term medical and psychosocial outcomes in congenital diaphragmatic hernia survivors. Arch Dis Child 2019;104:761–7. https://doi.org/10.1136/archdischild-2018-316091.

[126] Russell KW, Barnhart DC, Rollins MD, Hedlund G, Scaife ER. Musculoskeletal deformities following repair of large congenital diaphragmatic hernias. J Pediatr Surg 2014;49:886–9. https://doi.org/10.1016/j.jpedsurg.2014.01.018.

[127] Dillon PW, Cilley RE, Mauger D, Zachary C, Meier A, Altman RP, et al. The Relationship of Pulmonary Artery Pressure and Survival in Congenital Diaphragmatic Hernia. J. Pediatr. Surg., vol. 39, 2004, p. 307–12. https://doi.org/10.1016/j.jpedsurg.2003.11.010.

[128] de Lorimier A, Tierney D, Parker H. Hypoplastic lungs in fetal lambs with surgically produced congenital diaphragmatic hernia. Surgery 1967;62:12–7.

[129] Fauza DO, Tannuri U, Ayoub AAR, Capolozzi VL, Saldiva PHN, Maksoud JG. Surgically produced congenital diaphragmatic hernia in fetal rabbits. J Pediatr Surg 1994;29:882–6. https://doi.org/10.1016/0022-3468(94)90008-6.

[130] Costlow RD, Manson JM. The heart and the diaphragm: Target organs in herbicide-induced neonatal death. Teratology 1981;23.

[131] AYDIN E. Current Approach for Prenatally Diagnosed Congenital Anomalies That Requires Surgery. Turkiye Klin J Gynecol Obstet 2016;27:193–9. https://doi.org/10.5336/gynobstet.2016-53316.

[132] Varisco BM, Marotta M, Oria M, Aydin E, Schmidt R, Schroeder C, et al. Proteomic profiling of tracheal fluid in an ovine model of congenital diaphragmatic hernia and fetal tracheal occlusion.

Am J Physiol Cell Mol Physiol 2018;315:L1028–41. https://doi.org/10.1152/ajplung.00148.2018.

[133] Aydin E, Levy B, Oria M, Nachabe H, Lim F-Y, Peiro JL. Optimization of Pulmonary Vasculature Tridimensional Phenotyping in The Rat Fetus. Sci Rep 2019. https://doi.org/10.1038/s41598-018-37906-8.

[134] Aydin E, Joshi R, Oria M, Varisco BM, Lim FY, Peiro JL. Fetal tracheal occlusion in mice: a novel transuterine method. J Surg Res 2018. https://doi.org/10.1016/j.jss.2018.04.028.

[135] Tenbrinck R, Tibboel D, Galllard JLJ, Kluth D, Bos AP, Lachman B, et al. Experimentally induced congenital diaphragmatic hernia in rats. J Pediatr Surg 1990;25:426–9. https://doi.org/10.1016/0022-3468(90)90386-N.

[136] Aydın E, Yener E, Üstündağ N. Nitrofen kullanilarak oluşturulmuş konjenital diyafragma hernisi modelinde trakeal oklüzyonun akciğerlerin gelişimine etkisinin incelenmesi. Haseki Tip Bul 2016. https://doi.org/10.4274/haseki.2966.

[137] Mitchell LE, Adzick NS, Melchionne J, Pasquariello PS, Sutton LN, Whitehead AS. Spina bifida. Lancet 2017;6736:1885–95. https://doi.org/10.1016/S0140-6736(04)17445-X.

[138] Aydin E, Joshi R, Oria M, Varisco BM, Lim F-Y, Peiro JL. Fetal tracheal occlusion in mice: a novel transuterine method. J Surg Res 2018;229. https://doi.org/10.1016/j.jss.2018.04.028.

[139] Fung YC, Sobin SS. Elasticity of the pulmonary alveolar sheet. Circ Res 1972;30:451–69. https://doi.org/10.1161/01.res.30.4.451.

[140] Horton RF. Erosional development of streams and their drainage basins, hydrophysical approach to quantitive morphology. Nihon Ringakkai Shi/Journal Japanese For Soc 1955;37:79–82. https://doi.org/10.11519/jjfs1953.37.9_417.

[141] Strahler AN. Hypsometric (area-altitude) analysis of erosional topography. Bull Geol Soc Am 1952;63:1117–42. https://doi.org/10.1130/0016-7606(1952)63[1117:HAAOET]2.0.CO;2.

[142] Fenton BM, Zweifach BW. Microcirculatory model relating geometrical variation to changes in pressure and flow rate. Ann Biomed Eng 1981;9:303–21. https://doi.org/10.1007/BF02364653.

[143] Ley K, Pries AR, Gaehtgens P. Topological structure of rat mesenteric microvessel networks. Microvasc Res 1986;32:315–32. https://doi.org/https://doi.org/10.1016/0026-2862(86)90068-3.

[144] Hudetz A, Conger K, Halsey J, Pal M, Dohán O, Kovach A. Pressure Distribution in the Pial Arterial System of Rats Based on Morphometric Data and Mathematical Models. J Cereb Blood Flow Metab 1987;7:342–55. https://doi.org/10.1038/jcbfm.1987.72.

[145] VanBavel E, Spaan JA. Branching patterns in the porcine coronary arterial tree. Estimation of flow heterogeneity. Circ Res 1992;71:1200—1212. https://doi.org/10.1161/01.res.71.5.1200.

[146] Bertuglia S, Colantuoni A, Coppini G, Intaglietta M. Hypoxia- or hyperoxia-induced changes in arteriolar vasomotion in skeletal muscle microcirculation. Am J Physiol 1991;260:H362-72. https://doi.org/10.1152/ajpheart.1991.260.2.H362.

[147] Engelson ET, Skalak TC, Schmid-Schönbein GW. The microvasculature in skeletal muscle: I. Arteriolar network in rat spinotrapezius muscle. Microvasc Res 1985;30:29–44. https://doi.org/https://doi.org/10.1016/0026-2862(85)90035-4.

[148] Engelson ET, Schmid-Schönbein GW, Zweifach BW. The microvasculature in skeletal muscle. III. Venous network anatomy in normotensive and spontaneously hypertensive rats. Int J Microcirc Clin Exp 1985;4:229–48.

[149] Ganesan P, He S, Xu H. Development of an image-based network model of retinal vasculature. Ann Biomed Eng 2010;38:1566–85. https://doi.org/10.1007/s10439-010-9942-4.

[150] Vormberg A, Effenberger F, Muellerleile J, Cuntz H. Universal features of dendrites through centripetal branch ordering. PLOS Comput Biol 2017;13:e1005615.

[151] Yen RT, Zhuang FY, Fung YC, Ho HH, Tremer H, Sobin SS. Morphometry of cat's pulmonary arterial tree. J Biomech Eng 1984;106:131–6. https://doi.org/10.1115/1.3138469.

[152] Horsfield K. Morphometry of the small pulmonary arteries in man. Circ Res 1978;42:593–7. https://doi.org/10.1161/01.res.42.5.593.

[153] Singhal S, Henderson R, Horsfield K, Harding K, Cumming G. Morphometry of the human pulmonary arterial tree. Circ Res 1973. https://doi.org/10.1161/01.RES.33.2.190.

[154] Yen RT, Zhuang FY, Fung YC, Ho HH, Tremer H, Sobin SS. Morphometry of cat pulmonary venous tree. J Appl Physiol 1983;55:236–42. https://doi.org/10.1152/jappl.1983.55.1.236.

[155] Horsfield K, Gordon WI. Morphometry of pulmonary veins in man. Lung 1981;159:211–8. https://doi.org/10.1007/BF02713917.

[156] Kassab GS, Rider CA, Tang NJ, Fung YCB. Morphometry of pig coronary arterial trees. Am J Physiol - Hear Circ Physiol 1993. https://doi.org/10.1152/ajpheart.1993.265.1.h350.

[157] Jiang ZL, Kassab GS, Fung YC. Diameter-defined Strahler system and connectivity matrix of the pulmonary arterial tree. J Appl Physiol 1994. https://doi.org/10.1152/jappl.1994.76.2.882.

[158] Kassab GS, Imoto K, White FC, Rider CA, Fung YC, Bloor CM. Coronary arterial tree remodeling in right ventricular hypertrophy. Am J Physiol 1993;265:H366-75. https://doi.org/10.1152/ajpheart.1993.265.1.H366.

[159] Kassab GS, Lin DH, Fung YC. Morphometry of pig coronary venous system. Am J Physiol - Hear Circ Physiol 1994;267:H2100–H2113. https://doi.org/10.1152/ajpheart.1994.267.6.h2100.

[160] Peeters G, Debbaut C, Laleman W, Monbaliu D, Vander Elst I, Detrez JR, et al. A multilevel framework to reconstruct anatomical 3D models of the hepatic vasculature in rat livers. J Anat 2017;230:471–83. https://doi.org/10.1111/joa.12567.

[161] Wood S. A Morphological and Hemodynamic Analysis of Skeletal Muscle Vasculature. 2008.

[162] Lapi D, Di Maro M, Mastantuono T, Starita N, Ursino M, Colantuoni A. Arterial Network Geometric Characteristics and Regulation of Capillary Blood Flow in Hamster Skeletal Muscle Microcirculation. Front Physiol 2019;9:1953. https://doi.org/10.3389/fphys.2018.01953.

[163] Tarhuni M, Goldman D, Jackson D. Comprehensive In Situ Analysis of Arteriolar Network Geometry and Topology in Rat Gluteus Maximus Muscle. Microcirculation 2016;23. https://doi.org/10.1111/micc.12292.

[164] Hermán P, Kocsis L, Eke A. Fractal branching pattern in the pial vasculature in the cat. J Cereb Blood Flow Metab Off J Int Soc Cereb Blood Flow Metab 2001;21:741–53. https://doi.org/10.1097/00004647-200106000-00012.

[165] Lapi D, Marchiafava PL, Colantuoni A. Geometric characteristics of arterial network of rat pial microcirculation. J Vasc Res 2007. https://doi.org/10.1159/000109078.

[166] El-Bouri WK, Payne SJ. A statistical model of the penetrating arterioles and venules in the human cerebral cortex. Microcirculation 2016;23:580–90. https://doi.org/10.1111/micc.12318.

[167] Ii S, Kitade H, Ishida S, Imai Y, Watanabe Y, Wada S. Multiscale modeling of human cerebrovasculature: A hybrid approach using image-based geometry and a mathematical algorithm. PLOS Comput Biol 2020;16:1–28. https://doi.org/10.1371/journal.pcbi.1007943.

[168] Weibel ER. Fractal geometry: a design principle for living organisms. Am J Physiol 1991;261:L361-9. https://doi.org/10.1152/ajplung.1991.261.6.L361.

[169] West BJ, Goldberger AL. Physiology in Fractal Dimensions. Am Sci 1987;75:354–65.

[170] Lapi D, Marchiafava PL, Colantuoni A. Geometric Characteristics of Arterial Network of Rat Pial Microcirculation. J Vasc Res 2008;45:69–77. https://doi.org/10.1159/000109078.

[171] Bratu I, Flageole H, Laberge JM, Kovacs L, Faucher D, Piedboeuf B. Lung function in lambs with diaphragmatic hernia after reversible fetal tracheal occlusion. J Pediatr Surg 2004. https://doi.org/10.1016/j.jpedsurg.2004.06.024.

[172] Bratu I, Flageole H, Laberge JM, Possmayer F, Harbottle R, Kay S, et al. Surfactant levels after reversible tracheal occlusion and prenatal steroids in experimental diaphragmatic hernia. J Pediatr Surg 2001. https://doi.org/10.1053/jpsu.2001.20027.

[173] Hashim E, Laberge JM, Chen MF, Quillen EW. Reversible tracheal obstruction in the fetal sheep: Effects on tracheal fluid pressure and lung growth. J Pediatr Surg 1995. https://doi.org/10.1016/0022-3468(95)90015-2.

[174] Beck V, Davey MG, Mayer S, Froyen G, Deckx S, Klaritsch P, et al. A longer tracheal occlusion period results in increased lung growth in the nitrofen rat model. Prenat Diagn 2012;32:39–44. https://doi.org/10.1002/pd.2881.

[175] Roubliova X, Verbeken E, Wu J, Yamamoto H, Lerut T, Tibboel D, et al. Pulmonary vascular morphology in a fetal rabbit model for congenital diaphragmatic hernia. J Pediatr Surg 2004. https://doi.org/10.1016/j.jpedsurg.2004.03.049.

[176] Wu J, Ge X, Verbeken EK, Gratacós E, Yesildaglar N, Deprest JA. Pulmonary effects of in utero tracheal occlusion are dependent on gestational age in a rabbit model of diaphragmatic hernia. J Pediatr Surg 2001. https://doi.org/10.1053/jpsu.2002.29418.

[177] Yang J, Yu LX, Rennie MY, Sled JG, Henkelman RM. Comparative structural and hemodynamic analysis of vascular trees. AJP - Hear Circ Physiol 2010;298:H1249–59. https://doi.org/10.1152/ajpheart.00363.2009.

[178] Kool H, Mous D, Tibboel D, de Klein A, Rottier RJ. Pulmonary vascular development goes awry in congenital lung abnormalities. Birth Defects Res Part C - Embryo Today Rev 2014;102:343–58. https://doi.org/10.1002/bdrc.21085.

[179] Degenhardt K, Wright AC, Horng D, Padmanabhan A, Epstein JA. Rapid 3D phenotyping of cardiovascular development in mouse embryos by micro-CT with iodine staining. Circ Cardiovasc Imaging 2010;3:314–22. https://doi.org/10.1161/CIRCIMAGING.109.918482.

[180] Zhang C, Sun M, Wei Y, Zhang H, Xie S, Liu T. Automatic segmentation of arterial tree from 3D computed tomographic pulmonary angiography (CTPA) scans. Comput Assist Surg 2019. https://doi.org/10.1080/24699322.2019.1649077.

[181] Peiro JL, Oria M, Aydin E, Joshi R, Cabanas N, Schmidt R, et al. Proteomic Profiling of Tracheal Fluid in an Ovine Model of Congenital Diaphragmatic Hernia and Fetal Tracheal Occlusion. Am J Physiol Lung Cell Mol Physiol 2018. https://doi.org/10.1152/ajplung.00148.2018.

[182] Aydın E, Torlak N, Yildirim A, Bozkurt EG. Reversible Fetal Tracheal Occlusion in Mice: A Novel

Minimal Invasive Technique. J Surg Res 2021. https://doi.org/10.1016/j.jss.2020.11.080.

[183] Degenhardt K, Wright AC, Horng D, Padmanabhan A, Epstein JA. Rapid 3D phenotyping of cardiovascular development in mouse embryos by micro-CT with iodine staining. Circ Cardiovasc Imaging 2010;3:314–22. https://doi.org/10.1161/CIRCIMAGING.109.918482.

[184] Tran S, Shih L. Efficient 3D binary image skeletonization Efficient 3D binary image skeletonization. Comput Syst Bioinforma Conf 2005 Work Poster Abstr IEEE 2005:364–72. https://doi.org/10.1109/CSBW.2005.57.

[185] Counter WB, Wang IQ, Farncombe TH, Labiris NR. Airway and pulmonary vascular measurements using contrast-enhanced micro-CT in rodents. Am J Physiol Lung Cell Mol Physiol 2013;304:L831-43. https://doi.org/10.1152/ajplung.00281.2012.

[186] Lobregt S, Verbeek PW, Groen FCA. Three-Dimensional Skeletonization: Principle and Algorithm. IEEE Trans Pattern Anal Mach Intell 1980;PAMI-2:75–7. https://doi.org/10.1109/TPAMI.1980.4766974.

[187] Strahler AN. Quantitative analysis of watershed geomorphology. Eos, Trans Am Geophys Union 1957. https://doi.org/10.1029/TR038i006p00913.

[188] Horsfield K. Morphometry of the small pulmonary arteries in man. Circ Res 1978. https://doi.org/10.1161/01.RES.42.5.593.

[189] Lopes AA, Barreto AC, Maeda NY, Cícero C, Soares RPS, Bydlowski SP, et al. Plasma von Willebrand factor as a predictor of survival in pulmonary arterial hypertension associated with congenital heart disease. Brazilian J Med Biol Res 2011;44:1269–75. https://doi.org/10.1590/S0100-879X2011007500149.

[190] Rabinovitch M, Andrew M, Thom H, Trusler GA, Williams WG, Rowe RD, et al. Abnormal endothelial factor VIII associated with pulmonary hypertension and congenital heart defects. Circulation 1987;76:1043–52. https://doi.org/10.1161/01.CIR.76.5.1043.

[191] D. B, P.L. T, J. J, A. W, C. A, B. S, et al. High prevalence of elevated clotting factor VIII in chronic thromboembolic pulmonary hypertension. Thromb Haemost 2003.

[192] Song Y. Association study of circulating endothelial progenitor cells and plasma prostacyclin levels in pulmonary hypertension rats. Genet Mol Res 2014;13:438–44. https://doi.org/10.4238/2014.January.21.11.

[193] Zimmer J, Takahashi T, Hofmann AD, Puri P. Decreased Endoglin expression in the pulmonary vasculature of nitrofen-induced congenital diaphragmatic hernia rat model. Pediatr Surg Int 2017;33:263–8. https://doi.org/10.1007/s00383-016-4004-0.

[194] Kylhammar D, Hesselstrand R, Nielsen S, Scheele C, Rådegran G. Angiogenic and inflammatory biomarkers for screening and follow-up in patients with pulmonary arterial hypertension. Scand J Rheumatol 2018. https://doi.org/10.1080/03009742.2017.1378714.

[195] Alvarez DF, Huang L, King JA, Elzarrad MK, Yoder MC, Stevens T. Lung microvascular endothelium is enriched with progenitor cells that exhibit vasculogenic capacity. Am J Physiol - Lung Cell Mol Physiol 2008. https://doi.org/10.1152/ajplung.00314.2007.

[196] Good RB, Gilbane AJ, Trinder SL, Denton CP, Coghlan G, Abraham DJ, et al. Endothelial to Mesenchymal Transition Contributes to Endothelial Dysfunction in Pulmonary Arterial Hypertension. Am J Pathol 2015;185:1850–8. https://doi.org/10.1016/j.ajpath.2015.03.019.

[197] Rhodes CJ, Im H, Cao A, Hennigs JK, Wang L, Sa S, et al. RNA sequencing analysis detection of

a novel pathway of endothelial dysfunction in pulmonary arterial hypertension. Am J Respir Crit Care Med 2015;192:356–66. https://doi.org/10.1164/rccm.201408-1528OC.

[198] Safdar Z, Tamez E, Chan W, Arya B, Ge Y, Deswal A, et al. Circulating Collagen Biomarkers as Indicators of Disease Severity in Pulmonary Arterial Hypertension. JACC Hear Fail 2014. https://doi.org/10.1016/j.jchf.2014.03.013.

[199] Ranchoux B, Antigny F, Rucker-Martin C, Hautefort A, Péchoux C, Bogaard HJ, et al. Endothelial-to-mesenchymal transition in pulmonary hypertension. Circulation 2015;131:1006–18. https://doi.org/10.1161/CIRCULATIONAHA.114.008750.

[200] Short M, Nemenoff RA, Zawada WM, Stenmark KR, Das M. Hypoxia induces differentiation of pulmonary artery adventitial fibroblasts into myofibroblasts. Am J Physiol - Cell Physiol 2004. https://doi.org/10.1152/ajpcell.00169.2003.

[201] K. R. Clarke. Non-parametric multivariate analyses of changes in community structure. Aust J Ecol 1993.

[202] Mohseni-Bod H, Bohn D. Pulmonary hypertension in congenital diaphragmatic hernia. Semin Pediatr Surg 2007;16:126–33. https://doi.org/10.1053/j.sempedsurg.2007.01.008.

[203] Bentley MD, Ortiz MC, Ritman EL, Romero JC. The use of microcomputed tomography to study microvasculature in small rodents. Am J Physiol Regul Integr Comp Physiol 2002;282:R1267-79. https://doi.org/10.1152/ajpregu.00560.2001.

[204] Vickerton P, Jarvis J, Jeffery N. Concentration-dependent specimen shrinkage in iodine-enhanced microCT. J Anat 2013;223:185–93. https://doi.org/10.1111/joa.12068.